Journal of Bio- and Tribo-Corrosion (2024) 10:12
https://doi.org/10.1007/s40735-023-00811-3

Some Thoughts on Modeling Abrasion-Corrosion: Wear by Hard Particles in Corrosive Environments

Jiaren Jiang[1] · Md. Aminul Islam[1] · Yongsong Xie[1] · Margaret M. Stack[2]

Received: 7 September 2023 / Revised: 3 November 2023 / Accepted: 21 November 2023 / Published online: 23 January 2024

Abstract

Wear by hard particles can involve abrasion or erosion and is one of the most severe forms of wear. When a corrosive environment is present, the material loss rate can be significantly increased due to interactions (synergy) between the mechanical and chemical/electrochemical actions. In developing strategies for mitigating such adverse synergistic effect, it is important to understand the complex effect of various parameters on material loss under given tribocorrosion conditions. In this paper, a model is presented for wear-corrosion synergy in abrasive wear by hard particles applicable to many conditions in both the marine renewable (abrasion by high concentrations of large sand particles on tidal turbines) and extractive metallurgy (abrasive wear in mineral extraction). The mechanical wear loss is modeled based on the grooving mechanism (micro-cutting/micro-ploughing). Wear-enhanced corrosion is calculated from the fresh surface areas generated by grooving and the corresponding transient corrosion current. The concept of "corrosion-degraded layer" on the worn surface is introduced to account for the corrosion-enhanced wear; within this corrosion-degraded layer, the material loss rate is higher under the same mechanical wear conditions than in the material that is unaffected by corrosion. Based on the model, the effect of wear conditions on synergy in hard particle wear-corrosion has been discussed. The relative thickness of the corrosion-degraded layer to the depth of hard particle penetration (grooving) in the mechanical wear is found to be an important parameter in determining the relative severity of synergy in different tribocorrosion systems. Good qualitative agreement has been observed between the predictions and published experimental results obtained from a range of abrasion-corrosion and erosion-corrosion lab testing.

Keywords Abrasion-corrosion · Erosion-corrosion · Synergistic effect · Mathematical modeling · Tribocorrosion · Tidal turbines

Abbreviations

A_1, A_2	Volume of material pushed to the sides (ridges) of wear groove by the grooving action of a hard particle
A_a	Projected area of the activated wear surface by grooving (A_{ac})
$A_{a,\mathrm{act}}$	Total activated surface area on a unit wear surface created by all wear events within unit time
A_a,t	Total projected activated area created on unit apparent wear surface within the time interval between 0 and t_c
A_{ac}	New surface area created by sliding an abrasive particle over the wear surface (grooving) for a unit distance (activated surface area)
A_v	Volume of material displaced by the grooving action of a hard particle
F	Faraday's constant (= 96,485 C/mole)
f_r	Material removal factor that is defined as the ratio of material volume loss in a wear event divided by the volume of material displaced by the grooving action of a hard particle
f_r,d	Material removal factor within corrosion-degraded material layer
h_c	Average thickness of material loss due to corrosion within unit time

✉ Jiaren Jiang
jiaren.jiang@nrc-cnrc.gc.ca

[1] Mining Wear and Corrosion Laboratory, National Research Council Canada, 4250 Wesbrook Mall, Vancouver, BC V6T 1W5, Canada

[2] Department of Mechanical and Aerospace Engineering, University of Strathclyde, James Weir Building, 75 Montrose St, Glasgow G1 1XJ, UK

h_d Depth of corrosion-degraded material on the wear surface
h_w Penetration depth of abrasive particle tip into the wear surface
i_a Transient corrosion current density
$<i_a>$ Average corrosion current density on freshly exposed metal surface between two consecutive wear events from $t=0$ to $t=t_c$
i_{a0} Corrosion current density immediately following the depassivation of the metal surface by a wear event (the active corrosion current density)
I_c Total corrosion current on the unit apparent area of the wear surface
i_s Steady state corrosion current density
i^0_s Corrosion current density on material surface that is unaffected by wear
k Intermediate variable defined as $k = (i_{a0} - i_s)/(1-\sin\theta)\, i_s$
K_c Total material loss rate due to corrosion in the presence of wear
ΔK_c Wear-enhanced corrosion loss rate
K_c,sat Corrosion loss rate under saturated corrosion conditions
$\Delta K_c,sat$ Wear-enhanced corrosion loss rate under saturated corrosion conditions, i.e., when the whole wear surface is fully activated
K_{co} Corrosion-only material loss rate (corrosion in the absence of wear)
K_s Synergistic material loss rate
K_w Total material loss rate due to mechanical wear in the presence of corrosion
ΔK_w Corrosion-enhanced wear loss rate
K_{wc} Total material loss rate due to combined wear and corrosion
K_{wo} Wear-only material loss rate (wear in the absence of corrosion)
M Atomic weight (or molar mass) of the dissolving metal
n Number of abrasive particles in contact with a unit wear surface at any given time
r Radius of projected contact area between an abrasive particle and the wear surface
t_c Time interval between two successive wear events on the same location of the wear surface
V_d Volume of material within corrosion-degraded layer that is displaced by sliding an abrasive particle for a distance (in unit time) that is equal to v_x
V_{wo} Wear volume loss caused by the sliding (grooving) of n abrasive particles over the wear surface for a unit distance
v_x Velocity of abrasive particle traveling along the direction parallel to the wear surface
x Intermediate variable defined as $x=t_c/\tau$
z Average discharge valence of the metal for anodic reactions during corrosion
β Wear-enhancement factor, i.e., additional fraction of material to be removed, in the corrosion-degraded material layer by mechanical wear
θ Semi-inclusive angle of conical shaped abrasive particle tip
ρ Density of the corroding metal
τ Characteristic time for the decay of transient corrosion current at which time the corrosion current density has reduced to 63% of the initial value

1 Introduction

Wear by hard particles involves abrasion and erosion in which material loss is caused by contact between a hard particle and the surface of a solid material. Abrasion is the loss of material by the sliding or rolling mechanisms of hard particles over a surface, while erosion or erosive wear is caused by the impact of particles against a solid surface.

Tribocorrosion is a complex material degradation process due to the combined effect of chemical reaction (corrosion) and mechanical contact (wear). Extensive studies have been conducted on tribocorrosion in both abrasion [1–9] and erosion [10–39] conditions. In many cases, the total material loss due to combined corrosion and wear attack has been found to be greater, and often much greater, than the simple addition of losses from corrosion and wear if each acted independently. This phenomenon is referred to as synergism. In cases where the tribocorrosion layer provides protection to wear surface and reduces total material loss rate [40, 41], the process is termed antagonism.

Wear-corrosion synergy is commonly considered as being comprised of two components, i.e., (a) wear-enhanced corrosion which is the increased corrosion loss due to the mechanical actions of wear and (b) corrosion-enhanced wear which is the increased mechanical wear loss due to the presence of corrosion. Considerable efforts have been made to understand the mechanisms for these synergistic effects. However, the picture is still far from clear at the moment. From the literature, the possible mechanisms for synergism relevant to tribocorrosion in wear by hard particles can be summarized as follows.

(1) Mechanisms for wear-enhanced corrosion can generally be attributed to the mechanical activation of the wear surface and can be a result of one or more of the following reasons.

(1.1) Fresh metal surface is exposed to rapid corrosion after passive films are removed or damaged by the wear actions [26, 42–45].
(1.2) Impinging particles during erosion accelerate ion/mass transportation as a result of disruption and high turbulence of the solution boundary layer [25, 44–50].
(1.3) The real area of corrosion surface is increased due to a surface roughening effect [51, 52].
(1.4) Surface activity of the metal is enhanced in the strain hardened layer due to plastic deformation during wear, rendering the metal more anodic and more susceptible to corrosion [53–56].
(1.5) Local acidification in the erosion pits may occur which can accelerate corrosion rates and prohibit film formation [44, 45].

(2) On the other hand, corrosion-enhanced hard particle wear is far more complicated than wear-enhanced corrosion. Several mechanisms/theories have been proposed. However, so far no one seems to be universally applicable.

(2.1) Removal/dissolution of work-hardened surfaces by corrosion would expose the softer base metal and degrade the wear resistance of the material [44, 45, 55, 57, 58].
(2.2) Preferential corrosion of certain constituents/phases in non-uniform microstructures, such as in particulate reinforced materials where the matrix or the interface between the reinforcement hard particle and the matrix, would weaken the matrix support to the hard particles and lead to significant corrosion-enhanced wear [59–62]. Preferential corrosive attack at grain boundaries may result in grain weakening and eventual removal [44, 45].
(2.3) Anodic dissolution on the metal surface can cause the softening of the wear surface due to the so-called chemo-mechanical effect [63] and reduce the wear resistance of the material [20, 25, 31, 64].
(2.4) It was observed in erosion-corrosion test on stainless steels that platelets or lips formed during particle impingement were attacked/weakened by corrosion, making them more vulnerable to detachment by successive impingements [43]. This observation is similar to the mechanism proposed by Li et al. [65] who suggested that localized attack at disruptions in the surface oxide (caused by particle impacts) enhances the rate of crack growth, causing the flakes to become detached and leading to a higher erosion rate. This surface roughening effect has also been cited in several other publications as the mechanism for corrosion-enhanced erosion [51, 52, 66, 67]. These proposed mechanisms can largely be summarized as a result of increased number of stress-concentration defects due to localized corrosion [44, 45].
(2.5) It was proposed by Wood [44, 45] that corrosion may lower the fatigue strength of the metal and thus increase wear loss.

Wood and Hutton [44] summarized published erosion-corrosion testing data in the literature (including cavitation erosion and slurry erosion of various materials) and proposed a new format for analyzing the synergistic results. It was found that the ratio *S/C* of synergy (*S*) to pure corrosion rate (*C*) could be related to the ratio *E/C* of pure erosion rate (*E*) to pure corrosion rate (*C*) by the following expression:

$$\frac{S}{C} = A\left(\frac{E}{C}\right)^{B}$$

where *A* and *B* are constants. For results with medium *S/C* values (where synergistic effects are approximately 30% of the total erosion rate), $A = 0.148$ and $B = 1.277$. For high *S/C* values (where synergistic effects account for more than 60% of the total erosion rate), $A = 3.394$ and $B = 0.755$.

These relationships can be useful to the practicing engineers who have data of separate erosion (*E*) and corrosion rates (*C*) for a material so that synergistic erosion rate can be estimated/predicted for a particular application.

Since the late 1980s, extensive researches have been conducted on modeling synergism in tribocorrosion [68–77] to help understand and predict the evolution of tribocorrosion. Mischler et al. [73] and Landolt et al. [70] presented the first tribocorrosion model to describe the wear-enhanced corrosion component of synergy during sliding wear for passivating metals. The basic assumption in these works is that wear-enhanced corrosion is a result of repeated removal of passive films on the real area of contact. Analytical equations have been derived that can be used to analyze the effect of various parameters on synergy.

Stachowiak et al. [78, 79] and Ghanbarzadeh et al. [80] developed a model for sliding wear tribocorrosion systems by numerically calculating the components of synergy; the model applies contact mechanics to calculate the real area of contact and the corresponding electrochemical current transient at the asperity scale. Both corrosive and mechanical degradation mechanisms are applied on the asperity scale to predict material loss. The evolution of wear surface geometry is updated during the simulation.

Jiang et al. [81, 82] presented a phenomenological model for the synergistic effect in tribocorrosion. It was proposed that wear debris is formed by a low-cycle fatigue process involving the micro-crack initiation and propagation. In tribocorrosion conditions, corrosion or certain

"reactive species" in the environment can facilitate the initiation of micro-cracking and/or weaken the atomic bonding at the crack tip, accelerating the wear debris generation and hence increasing the wear rate. This is in line with the observation by Rajahram et al. [43] who noticed in an erosion-corrosion study of stainless steels that corrosion preferentially attacks the roots of platelets or lips formed during particle impingement, leading to their more rapid detachment/removal by successive impingements. The model by Jiang et al. [81, 82] includes many material parameters that are difficult or impossible to obtain and this provides challenges to mathematical modeling of this area. However, it is useful for analyzing important factors that can affect synergy in a given tribosystem and how.

Based on the concept of chemo-mechanical effect [63], Lu et al. [20] developed an erosion-corrosion model that attributes corrosion-enhanced erosion to the softening of the wearing surface under the influence of anodic corrosion current flow [25, 64]. It was found that erosion rates in corroding slurry are a linear function of logarithmic corrosion rate (anodic current density).

From a practical application perspective, numerical simulation has become a useful tool for predicting "safe" and "unsafe" zones in an engineering system where most severe damage is expected so that appropriate mitigation strategies can be applied to prevent unexpected situations from occurring. A number of researches have been devoted to modeling and simulating erosion-corrosion in pipes and pipe elbows under different conditions [28, 83–87]. Although the emphases, objectives, and situations are different among the various researches, the basic methodologies are similar. By applying different theories and/or empirical formula, expressions are proposed for the correlations between various components of erosion-corrosion synergy (pure erosion, pure corrosion, erosion-enhanced corrosion, and corrosion-enhanced erosion) and erosion-corrosion conditions. Then, computational fluid dynamics (CFD) is used to obtain detailed parameters that are required for predicting the evolution of erosion and corrosion at locations of interests. For example, Stack et al. [84] adopted the solid particle erosion model by Sundararajan [88] to predict the erosion rates and a range of corrosion models to predict the corrosion rates. The total material wastage was then estimated by combining the erosion and corrosion rates. Material wastage maps as well as maps for transitions between erosion-corrosion regimes were constructed for a pipe bend. This work showed that it is possible to identify erosion-corrosion mechanistic regimes on real components under nominally similar fluid flow conditions.

It should be pointed out that in references [84–86], the total erosion-corrosion loss was obtained by simply calculating and adding together losses due to pure erosion and pure corrosion, respectively, while the synergistic effect had been neglected.

When developing strategies for mitigating adverse wear-corrosion synergistic effect, it is important to understand the complex effects of various operation parameters on material loss under given tribocorrosion conditions. Properly designed systematic experimental studies can help to uncover some of these effects. However, it is difficult, if not impossible, to experimentally study all possible situations that can be encountered in practice. On the other hand, modeling is a technique that describes the relationship of phenomena to each other, with the assumption that the relationship extends past the measured values. While it does not attempt to explain why the variables interact the way they do, modeling can provide insights that go beyond what is already known or can be achieved from direct observations; thus modeling is a powerful tool to expand our knowledge of interactions of the phenomena and develop appropriate hypotheses. In this paper, a mathematical model is presented for wear-corrosion synergism in wear by hard particles. Based on the model, the effect of major wear conditions on synergy in hard particle wear-corrosion will be discussed and compared with experimental results from the literature.

2 Model for Synergism in Wear by Hard Particles

2.1 General Considerations/Basic Assumptions

Consider a unit area of the wear surface being worn by hard particles as schematically shown in Fig. 1a.

Assume that the abrasive tip causing the hard particle wear has a conical shape with an apex inclusive angle of 2θ, Fig. 1b. During the wear process, the conical abrasive tip penetrates into the wear surface by a depth of h_w under mechanical loading and makes a projected circular (semi-circular when moving) contact on the top wear surface with a radius of r. The abrasive particle travels at a velocity of v_x in the direction parallel to the wear surface.

During the wear process, corrosion occurs on the metal surface, dissolving a layer with a thickness of h_c within a given time (unit time in the context of the current paper). It should be noted that h_c (Fig. 1b) represents a conceptual corrosion "layer." Physically, it is a cumulative result of metal dissolution (corrosion), atom by atom, from the wearing surface. When analyzing the material loss due to mechanical wear (pure wear and corrosion-enhanced wear), its physical thickness can be treated as equal to zero.

When an abrasive particle slides over the wear surface, a wear groove is formed and fresh metal surface is exposed to active corrosion. As schematically illustrated in Fig. 2, the activated surface area, A_{ac}, created by sliding of the hard

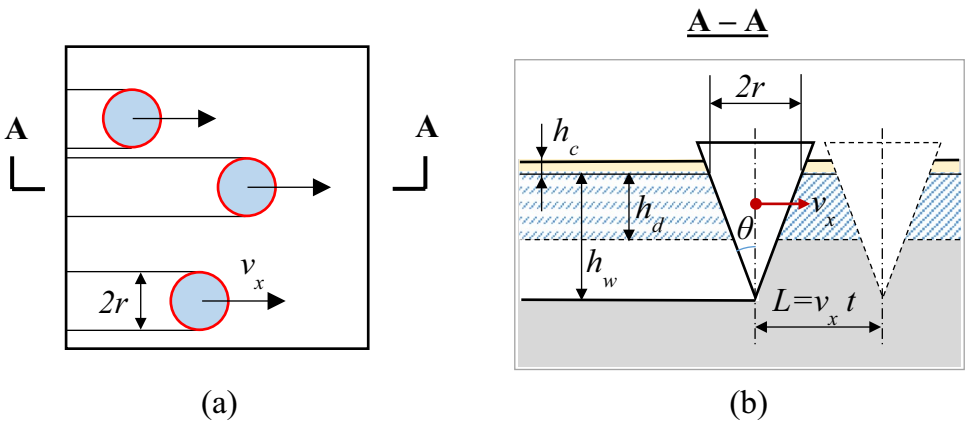

Fig. 1 Schematic diagrams showing **a** top view of a unit area of wear surface being worn by hard particles and **b** cross-section of a wear groove

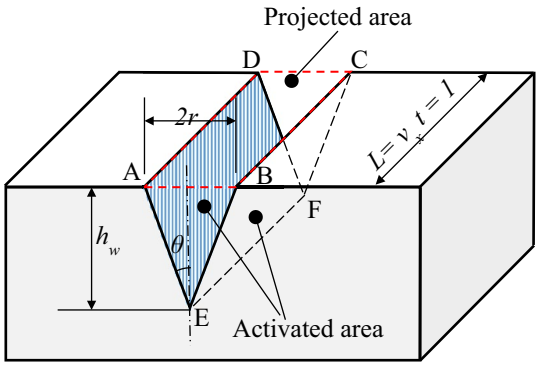

Fig. 2 Schematic diagram showing the activated surface area (A_{ac}) and the projected area (A_a) where A_{ac} = AEFD + BEFC and A_a = ABCD

particle for a unit distance, $L = 1$, is equal to the shaded area on the groove face (AEFD + BEFC) and can be calculated by

$$A_{ac} = \frac{2r}{sin\theta} \cdot 1 = \frac{2h_w}{cos\theta} = \frac{A_a}{sin\theta} \tag{1}$$

The projected area (ABCD) of the activated wear surface, A_a, is given by

$$A_a = 2r \cdot 1 = 2h_w tan\theta \tag{2}$$

In all the following analyses, a unit apparent area of the wear surface will be considered.

As discussed in the Introduction, mechanisms for corrosion-enhanced wear are still not well understood. It is likely that the actual damage mechanisms may depend on conditions in individual tribosystems. However, it can be envisaged that in the tribocorrosion process, a certain volume of the solid material in the surface and/or subsurface region is somehow damaged/degraded due to the presence of the corrosive medium, making it more vulnerable to removal by the mechanical wear event. In other words, when wear occurs in or involving this degraded/weakened material, a larger volume of material is removed/worn than that if wear occurs in non-degraded state of the same material. It is this additional material loss that leads to the corrosion-enhanced wear. To account for this effect, this volume of affected/weakened material near the wear surface is defined as the corrosion-degraded material. The depth of the corrosion-degraded material can be defined by h_d, Fig. 1b.

2.2 Wear-Only Loss Rate, K_{wo}

Assume n abrasive particles are in contact with the unit wear surface at any given time. The wear volume loss, V_{wo}, caused by the sliding of the n particles for a unit distance can be calculated by

$$V_{wo} = n(rh_w)f_r = nh_w^2 tan\theta f_r \tag{3}$$

where the abrasive penetration depth, h_w, is related to the half-width of the formed groove, r, by (Fig. 1)

$$r = h_w tan\theta$$

f_r is the material removal factor that is defined as the ratio of material volume loss in a wear event divided by the volume of material displaced by the sliding action of a hard particle, A_v, Fig. 3, i.e.,

$$f_r = \frac{A_v - (A_1 + A_2)}{A_v}$$

This factor is introduced because the material displaced from the wear groove by the sliding of a hard particle may not be completely removed in a single wear event [89–93].

The wear-only wear rate (volume loss per unit time), K_{wo}, is obtained by multiplying V_{wo} by the sliding/scratching velocity, v_x

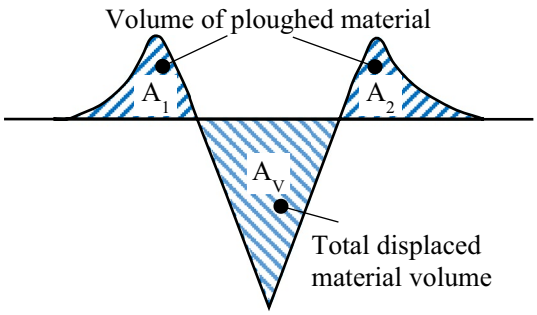

Fig. 3 Schematic diagram showing the definition of material removal factor, f_r

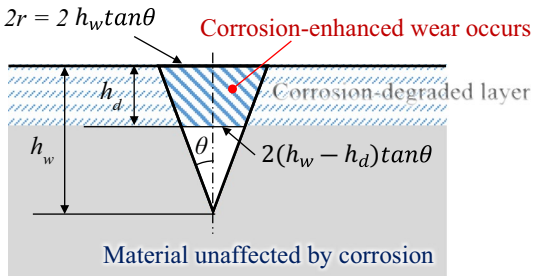

Fig. 4 Diagram showing the region of material where corrosion-enhanced wear occurs

$$K_{wo} = V_{wo}v_x = nv_x h_w^2 tan\theta f_r \tag{4}$$

2.3 Corrosion-Enhanced Wear Rate, ΔK_w

Corrosion-enhanced wear occurs within the corrosion-degraded material volume (layer), h_d. For the same volume of material that is displaced by the sliding of a hard abrasive particle over the wear surface (the mechanical action), material loss in the corrosion-degraded material layer is usually greater than that in the material that has not been affected by corrosion. If the ratio of additional volume loss within the corrosion-degraded layer to the volume loss when wear occurs in the same material unaffected by corrosion is equal to β, then the material removal fraction in the corrosion-degraded material layer (volume), $f_{r,d}$, is related to that in the virgin material f_r by Eq. (5),

$$f_{r,d} = (1+\beta)f_r \tag{5}$$

It should be noted that the factor β in Eq. (5) is positive in tribocorrosion systems with synergistic effect and is negative in tribosystems showing antagonistic effect. In the material that is not affected by corrosion, $\beta = 0$.

Referring to Fig. 4, the corrosion-enhanced wear loss rate, ΔK_w, can be obtained by calculating the volume of material (V_d) within this corrosion-degraded layer (h_d) that is displaced by sliding a hard particle for a distance (in unit time) of v_x multiplied by the extra material removal factor for corrosion-degraded material (i.e., βf_r, Eq. (5)) and the number of wear events (i.e., the number of contacting abrasive particles, n) on a unit area of the wear surface:

$$V_d = v_x\left[(h_w - h_d)tan\theta + h_w tan\theta\right]h_d$$

and

$$\begin{aligned}\Delta K_w &= n[V_d(\beta f_r)] \\ &= nv_x(\beta f_r)h_d(2h_w - h_d)tan\theta \\ &= \beta K_{wo}\left[1-\left(1-\frac{h_d}{h_w}\right)^2\right]\end{aligned} \tag{6}$$

The total material loss rate due to mechanical wear, K_w, is equal to the sum of wear-only rate, K_{wo}, and the corrosion-enhanced wear rate, ΔK_w, i.e.,

$$\begin{aligned}K_w &= K_{wo} + \Delta K_w \\ &= K_{wo}\left\{1+\beta\left[1-\left(1-\frac{h_d}{h_w}\right)^2\right]\right\}\end{aligned} \tag{7}$$

2.4 Total Corrosion, K_c, and Wear-Enhanced Corrosion, ΔK_c

Consider a given location on the wear surface. During wear, the surface is dynamically activated by wear events followed by repassivation between two successive wear events at the same location. Thus, at any given time, the wear surface can be identified by two types of regions: (i) where activated metallic surface is exposed (including areas being repassivated) and (ii) where the surface is fully repassivated and/or corrosion occurs at steady state rate. It should be highlighted that the "repassivated" region on the wearing surface may be different from that under static corrosion before wear because the wear surface is being work hardened.

Researches [94, 95] have shown that, when tensile test is conducted on a specimen immersed in a corrosive solution, corrosion of the specimen is accelerated and the corrosion rate increment (current, ΔJ_{max}) is proportional to straining rate, $\dot{\varepsilon}$:

$$\Delta J_{max} = K\dot{\varepsilon}^{\alpha}$$

where K and α are constants.

This phenomenon can largely be explained by the fact that new/fresh (non-passivated) metal surface is created by the plastic deformation and the freshly exposed metal surface area increases with the increase in strain rate, $\dot{\varepsilon}$,

leading to higher corrosion rate. Similar processes can be expected during tribocorrosion where fresh metal surface area is constantly created by wear.

2.4.1 Total Corrosion Rate During Wear, K_c

On each individual activated surface area by one wear event, A_{ac}, the transient corrosion current density, i_a, decreases with time from high values on the freshly exposed surface toward steady state value, i_s. The activated corrosion area A_{ac} and the corresponding projected area A_a have been provided in eqs. (1) & (2).

Discrete activation of the wear surface dynamically occurs due to wear events over different locations of the wear surface. At a steady state of wear, on average (statistically), there will be a certain fraction of the apparent area of the wear surface that is in the activated state; this fraction of activated area, i.e., the total activated surface area on a unit wear surface, created by all the wear events within unit time, $A_{a,act}$, can be calculated by

$$A_{a,act} = nA_a v_x \tag{8}$$

Note: A_a is the projected area created by sliding a single abrasive particle against the wear surface for a unit distance ($L = 1$). Multiplying A_a by ($v_x/L = v_x$) converts the unit for $A_{a,act}$ from per unit sliding distance to per unit time.

The rest of the wear surface, $1-A_{a,act}$, is corroded at the steady state corrosion current density, i_s. The total corrosion current on the unit apparent area of the wear surface, I_c, within unit time is the sum of corrosion currents on activated surface areas (repassivation) and on areas at steady state corrosion. I_c can be calculated by

$$\begin{aligned} I_c &= Repassivationcorrosion + Steadystatecorrosion \\ &= nA_{ac}v_x\left(\frac{1}{t_c}\int_0^{t_c} i_a dt\right) + \left(1 - nA_a v_x\right)i_s \end{aligned} \tag{9}$$

In the above equation, t_c is the time interval between two successive wear events on the same location of the wear surface within which time the activated surface undergoes repassivation. The term before the first set of parentheses is the total activated (roughened real) surface area of the metal by the grooving event within the unit time.

The total corrosion rate (on unit apparent surface area within unit time), K_c, during wear-corrosion is related to the corrosion current, I_c, by the Faraday's law and is given by (applying eqs. (1) and (2) for A_{ac} and A_a):

$$\begin{aligned} K_c &= \frac{M}{z\rho F} I_c \\ &= \frac{M}{z\rho F}\left[\frac{nA_{ac}v_x}{t_c}\int_0^{t_c} i_a dt + \left(1 - nA_a v_x\right)i_s\right] \\ &= \frac{M}{z\rho F}\left\{\frac{2nv_x h_w}{cos\theta}\left[\frac{1}{t_c}\int_0^{t_c} i_a dt - sin\theta i_s\right] + i_s\right\} \end{aligned} \tag{10}$$

where M—atomic weight (or molar mass) of the dissolving metal; z—average discharge valence of the metal for anodic reactions during corrosion; ρ—density of the corroding metal; and F—Faraday's constant (= 96,485 C/mole).

Equation (10) is valid under the following conditions:

$$1 - nA_a v_x > 0 \tag{11}$$

i.e., when the projected total activated area is less than the total apparent wear surface area so that there are some areas on the wear surface that are undergoing steady state corrosion (i_s).

When $1 - nA_a v_x \le 0$, the whole apparent area of the wear surface is being activated at all the times, with different locations of the surface being at different stages of repassivation at any given time. We can regard this condition as saturated corrosion. Under such conditions, there is no apparent area of the wear surface that has reached the steady state corrosion (i_s) before being attacked (re-activated) again by the next wear event and the second term on the second line of Eq. (10) becomes zero, i.e., $(1 - nA_a v_x)i_s = 0$. Equation (10) is now reduced to

$$K_{c,sat} = \frac{M}{z\rho F}\frac{nv_x}{t_c}\frac{2h_w}{cos\theta}\int_0^{t_c} i_a dt \tag{12}$$

where $K_{c,sat}$ is the corrosion loss rate in saturated corrosion condition.

The repassivation time interval, t_c, is related to wear parameters by the following equation (eq. (43), Appendix A):

$$t_c = \frac{1}{2nv_x h_w tan\theta} \tag{13}$$

2.4.2 Wear-Enhanced Corrosion Rate, ΔK_c

Applying the Faraday's law, the corrosion-only rate, K_{co}, is calculated by

$$K_{co} = \frac{M}{z\rho F} i_s^0 \tag{14}$$

i_s^0 in Eq. (14) is the corrosion current density on the surface of the same material before wear test. This may be different from the corrosion current density, i_s, on a wear surface outside activated surface areas because worn surface may have higher free energy due to plastic deformation [51–54].

For simplicity, the difference between these two values will be neglected in the following analysis, i.e., it is assumed that $i_s^0 \cong i_s$ and

$$K_{co} \approx \frac{M}{z\rho F} i_s \tag{15}$$

By applying eqs. (10) and (15), the wear-enhanced corrosion, ΔK_c, can be related to wear-only loss rate (Eq. (4)), K_{wo}, by

$$\Delta K_c = K_c - K_{co} = \frac{M}{z\rho F} 2\left(\frac{n v_x K_{wo}}{f_r \sin\theta \cos\theta}\right)^{1/2} \left[\frac{1}{t_c}\int_0^{t_c} i_a dt - \sin\theta i_s\right] \tag{16}$$

In Eq. (16), the first term in the square bracket is essentially the average corrosion current density, $< i_a >$, on the freshly exposed metal surface between two consecutive wear events from $t = 0$ to $t = t_c$:

$$\frac{1}{t_c}\int_0^{t_c} i_a dt = < i_a > \tag{17}$$

Under fully activated/saturated corrosion conditions, the wear-enhanced corrosion is related to wear intensity, K_{wo}, by applying eqs. (2), (4), (12), (13), and (15):

$$\Delta K_{c,sat} = K_{c,sat} - K_{co} = \frac{M}{z\rho F}\left[\frac{4 n v_x K_{wo}}{f_r cos\theta}\int_0^{t_c} i_a dt - i_s\right] \tag{18}$$

2.5 Synergy, K_s, and Total Wear-Corrosion Loss Rate, K_{wc}

The total material loss rate in the combined wear-corrosion conditions, K_{wc}, can be expressed in one of the two forms as shown in eqs. (19) & (20), respectively:

$$K_{wc} = K_{wo} + K_{co} + K_s \tag{19}$$

or

$$K_{wc} = \left(K_{wo} + \Delta K_w\right) + \left(K_{co} + \Delta K_c\right) = K_w + K_c \tag{20}$$

where

$$K_w = K_{wo} + \Delta K_w \tag{21}$$

$$K_c = K_{co} + \Delta K_c \tag{22}$$

K_{wc} = total wear-corrosion loss rate, K_{wo} = wear-only loss rate (wear in the absence of corrosion), K_{co} = corrosion-only loss rate (corrosion in the absence of wear), K_s = synergy, ΔK_w = corrosion-enhanced wear, ΔK_c = wear-enhanced corrosion, K_c = total corrosion rate in the presence of wear, and K_w = total wear rate in the presence of corrosion.

The various components of wear-corrosion synergy have been derived in Sects. 2.2-2.4. Then, the synergy, K_s, and the total wear-corrosion loss rate, K_{wc}, can be obtained by the following relations, eqs. (23) and (24):

$$K_s = \Delta K_w + \Delta K_c \tag{23}$$

$$K_{wc} = K_w + K_c, \tag{24}$$

where K_w and K_c are given in Eq. (7) and Eq. (10), while ΔK_c and ΔK_w are provided in Eqs. (16) and (6), respectively.

3 Discussion

The wear-only material loss rate, K_{wo}, is a reflection of the severity of mechanical wear conditions in a given wear-corrosion system and will be referred to as wear intensity in the following discussions.

Equations (6) and (16) show that wear intensity, K_{wo}, is one of the major factors affecting both components of synergy, i.e., the corrosion-enhanced wear, ΔK_w, and wear-enhanced corrosion, ΔK_c. It should be noted that, in addition to the explicit inclusion of the term K_{wo} in these equations, the parameters n and v_x are directly related to the wear intensity (Eq. (1)). The repassivation time, t_c, is also indirectly influenced by the wear intensity (Eq. (13)).

The following discussions will focus on the effect of wear intensity on the various components of synergy and comparison of the model predictions with data published in the literature. Before diving into those details, it is useful to first clarify where or under what conditions the model can be applied.

3.1 The Applicability of the Model

The mechanical wear loss in this model is based on the micro-cutting and micro-ploughing (the material removal factor, f_r) mechanisms by the sliding of a hard abrasive particle over the wear surface. Therefore, strictly speaking, it would apply to two-body abrasion only since other mechanisms such as rolling and rolling-sliding also contribute to the total wear loss in 3-body abrasion. Nevertheless, it is commonly observed that cutting and ploughing are the dominant mechanisms in 3-body abrasion and account for the majority of the wear losses in non-brittle materials. Therefore, the general trends derived from this model should be applicable for 3-body abrasion as well.

On the other hand, slurry erosion by hard particles is superficially a completely different process from abrasion. One important difference is that, during erosion, strain rate in the affected material can be considerably higher than that in abrasion. However, according to Johnson [96], our

knowledge of inelastic contact stresses under static conditions can be used to investigate impact behavior for "moderate impact velocities (up to 500 m/s, say)." Another obvious difference is that hard particles in erosion impact the wear surface at some oblique angle and the grooving geometries are not constant but vary during each single impact event. In addition, during erosion, repeated indentation is often observed, particularly at high impingement angles. But, as in the case for abrasion, grooving (micro-cutting/micro-ploughing) usually makes one of the most important contributions to the total material loss during erosion of non-brittle materials. This is particularly true for erosion at low to medium impingement angles. In fact, our previous modeling and simulation work [97] on particle trajectories in a laboratory slurry jet erosion tester have shown that even at a nominal 90° impingement angle, the majority of the erodent particles actually impact the wear surface at much lower angles, mostly below 60°. Since the main objective of the current model is to uncover the important relations between wear-corrosion synergism behavior of a material and the various influencing factors rather than to provide accurate predictions, it is not unreasonable to extend the application of this model to qualitatively explain erosion-corrosion phenomena observed in most slurry erosion.

To apply the current model for erosion-corrosion analysis, the relative particle sliding velocity over the wear surface, v_x, is the horizontal component of the impact velocity, v. The depth of wear penetration, h_w, and the radius of indentation, r, in erosion are not constant but vary with time or distance from the incident point of contact to the point where the abrasive particle stops moving or leaves the contact surface. In such cases, the average values of the erosion grooves formed during a single impact erosion event can be used for the corresponding geometrical parameters (penetration depth, h_w, and radius of indentation, r). These values can be estimated/derived from the solid particle erosion models by Finnie [98, 99] and Bitter [100, 101]. In addition, the material removal factor (f_r) can be related directly to the deformation wear factor as proposed by Bitter [100, 101] which is defined as energy needed to remove a unit volume of material from the body surface by deformation wear.

Based on the above argument, both abrasion-corrosion and erosion-corrosion data published in the literature will be used to illustrate the validity of the model.

3.2 Wear-Enhanced Corrosion as a Function of Wear Intensity

In studies on sliding wear of a CoCrMo alloy against a ceramic ball in phosphate-buffered saline solution, Ghanbarzadeh et al. [80, 102] showed that the total corrosion increases linearly with the mechanical wear rate (i.e., wear intensity). Corrosion-enhanced wear also has a linear correlation with mechanical wear loss.

Passive film dynamics and transient current in corrosion for passivating metals have been extensively studied and there is a vast literature, e.g., compilations can be found in general textbooks such as those by Kaesche and Marcus [103, 104]. There have also been studies on the measurement [105–107] and modeling [80, 102, 108] of corrosion and corrosion current decay during tribocorrosion test. Dalbert et al. [107] used an exponential current decay function to approximate the response to film removal in tribocorrosion experiments and showed a good fit to experimental curves. Mary et al. [109] in recent work used similar approach by involving two exponential functions with two different time constants, one representing film nucleation on a bare metal surface and the other for film growth. Ghanbarzadeh et al. [80, 102] adopted a different approach in their deterministic tribocorrosion model by assuming the repassivation to occur at a series of discrete locations (real areas of contact at asperities) and then summing the contributions of all locations at the wear interface to obtain the complete/total corrosion current [102]. All the depassivation/repassivation studies so far such as those quoted above have been focused on passivating metals. In general, for passivating metals, the corrosion current decays rapidly from a maximum value on freshly depassivated/activated metal surface to a near-zero value on fully repassivated surface.

For non-passivating metals, there are no reported studies that can be applied to describe the transient corrosion current on fresh/depassivated metal surface exposed by wear event. Based on the fundamental principles of corrosion, there are two types of corrosion transient kinetics for corrosion on a freshly activated (depassivated) metal surface such as that exposed by hard particle wear, i.e., activation controlled and mass transport controlled.

3.2.1 Activation Controlled Corrosion Situation

In activation controlled corrosion, corrosion rate is controlled by the rate of charge transfer at the metal surface in the oxidation and reduction reactions, while the migration of reactants and products of the corrosion process to and from the metal surface is much faster and does not affect the corrosion rate. Under such conditions, the corrosion rate or corrosion current on the depassivated metal surface does not change with time and will be the same as that in the surrounding non-activated area. The first term in the square bracket of Eq. (16) will be equal to a constant steady state corrosion rate, i_s, i.e.,

$$< i_a >= \frac{1}{t_c} \int_0^{t_c} i_a dt = i_s \tag{25}$$

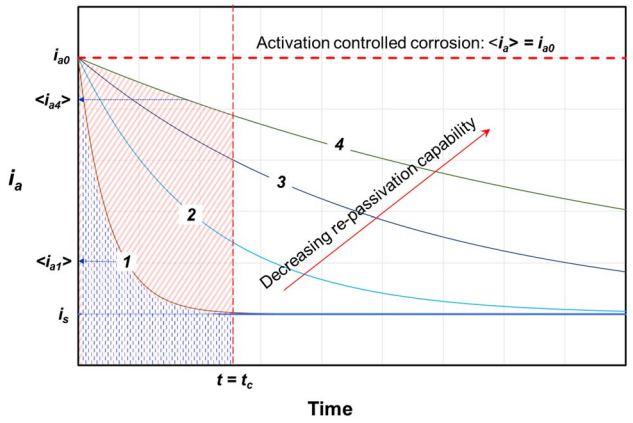

Fig. 5 Schematic diagram showing the repassivation behavior of metals with different passivation/repassivation capabilities

Equation (16) is reduced to the following for activation controlled corrosion:

$$\Delta K_c = \frac{M}{z\rho F} 2\left(\frac{nv_x K_{wo}}{f_r sin\theta cos\theta}\right)^{1/2} (1 - sin\theta)\, i_s \tag{26}$$

Equation (26) shows that if the metal corrosion is controlled by activation, then the wear-enhanced corrosion is due to the roughening (grooving) effect only; the corroding surface area is increased by a factor of $(1-sin\ \theta)$ which is determined/affected by the geometry of the abrading particle. Sharp or angular hard particles are expected to generate higher wear-enhanced corrosion.

3.2.2 Situations Where Corrosion is Controlled by Mass Transport

In conditions where corrosion is controlled by mass transport, surface concentration of a reactant is different from that in the bulk medium. The rate of charge transfer reaction at the interface depends not only on the electric potential but also on the concentration of reacting species prevailing at the electrode surface. Some of the controlling steps can include the dissipation of metal ions away from the interface or the diffusion of reducing agent such as oxygen toward the interface. In any case, the gradient of the reactant concentration near the interface, and hence the corrosion rate or corrosion current, i_a, is the highest immediately following the depassivation of the metal surface by a wear event ($i_a = i_{a0}$ at $t = 0$). The corrosion current, i_a, will decrease gradually with time as the concentration of reactants builds up or depletes near the interface that leads to the decrease in concentration gradient. Given sufficient time, the corrosion current will reach the steady state value, i_s.

Based on the above discussions, the variation of repassivation corrosion current, i_a, as a function of time on depassivated surface following a wear event can be qualitatively described by Fig. 5 for metals with different repassivation behaviors. As discussed above, there is essentially no repassivation if the corrosion reaction is activation controlled, in which case $< i_a > = i_{ao} = i_s$. For materials with strong passivation capabilities such as passivating metals, corrosion current decays rapidly to reach the steady state value within very short time (e.g., case 1 in Fig. 5). With decrease in the repassivation capability, the speed of corrosion current decay decreases (e.g., from case 1 to case 4 in Fig. 5). Under the same wear conditions, the average repassivation corrosion current, $< i_a >$, is expected to be much lower for metals with high repassivation capability than those that are difficult to passivate/repassivate, e.g., $< i_{a1} >$ for case 1 vs. $< i_{a4} >$ for case 4 in Fig. 5.

It should be pointed out that the schematic diagrams in Fig. 5 compare situations where the materials have the same active corrosion current, i_{a0}, and steady state corrosion current, i_s. This is applicable when analyzing the synergy response of a given material in the same corrosion medium. For materials with different corrosion resistance and repassivation capabilities, the absolute values of i_{a0} and i_s may be different. Nevertheless, the general trends depicted in Fig. 5 and Eq. (16) can still be applied for qualitatively analyzing the effects of various factors, including electrochemical corrosion behaviors, on the wear-enhanced corrosion component of synergy.

According to Eq. (16) (the 2nd term), wear-enhanced corrosion is also affected by the steady state corrosion current, i_s. For metals having very high steady state corrosion current, the wear-enhanced corrosion may not be significant because the whole surface is being actively corroded no matter whether or not the surface is attacked by mechanical wear.

In addition to the repassivation capability or corrosion resistance of the material, the average repassivation corrosion current (the first term in the square bracket of Eq. (16)) is also affected by the critical repassivation time, t_c. According to Eq. (13), the time for repassivation, t_c, decreases continuously with the increase in wear intensity (i.e., n, h_a and/or v_x). From the schematic diagrams in Fig. 5, the average corrosion current $< i_a >$ will increase with the decrease in t_c (integration within the higher current range) or with the increase in the wear intensity.

Overall, terms within the square bracket of Eq. (16) increase with the increase in the wear intensity. As a result, the wear-enhanced corrosion, ΔK_c, is also expected to increase with wear intensity. Data from the literature to be presented below (Fig. 7) do support this postulation.

To obtain a more visual general trend for the variation of wear-enhanced corrosion, the following special case will be considered. Assume that the decay of transient corrosion current can be approximated by an exponential

function as has been observed in stainless steels [107, 109], pure iron [95], and Al–Mg alloys [110]:

$$i_a = \left(i_{a0} - i_s\right) \exp\left(-\frac{t}{\tau}\right) + i_s \tag{27}$$

where τ is a characteristic time for the decay of transient corrosion current. Higher values of τ mean slower repassivation or poorer repassivation capability.

Applying Eq. (27), the wear-enhanced corrosion can be calculated by (eq. (50), Appendix B)

$$\Delta K_c = \frac{M}{z\rho F}\left[\frac{(1-sin\theta)i_s}{\tau sin\theta}\right] g(x) \tag{28}$$

where

$$g(x) = \frac{1}{x}\left\{\frac{1}{x}k\left[1 - \exp(-x)\right] + 1\right\} \tag{29}$$

$$x = \frac{t_c}{\tau} \tag{30}$$

and

$$k = \frac{\left(i_{a0} - i_s\right)}{(1 - sin\theta)i_s} \tag{31}$$

Under high wear intensity conditions where the whole wear surface is fully activated all the time, i.e., under saturated corrosion conditions, the wear-enhanced corrosion, $\Delta K_{c,sat}$, can be expressed by (eq. (52), Appendix B)

$$\Delta K_{c,sat} = \frac{M}{z\rho F}\frac{i_s(1-sin\theta)}{sin\theta} m(x) \tag{32}$$

where

$$m(x) = \left\{\frac{1}{x}k[1 - \exp(-x)] + 1\right\} \tag{33}$$

Equation (28) is applicable when $t_c > 1$ at relatively low wear intensity levels, while Eq. (32) applies when $t_c \leq 1$ for saturated corrosion situation.

When wear is very severe and/or if the metal is difficult to repassivate (with high characteristic repassivation time τ), the value t_c/τ becomes very small ($t_c << \tau$), i.e., $\times \rightarrow 0$ and the whole wear surface is constantly being corroded at the activated corrosion current rate, i_{ao}. This is the limiting condition where the wear-enhanced corrosion reaches the maximum rate:

$$\begin{aligned}\Delta K_{c,sat,lim} &= \frac{M}{z\rho F}\frac{1}{sin\theta}\left[(i_{a0} - i_s) + i_s(1 - sin\theta)\right] \\ &= \frac{M}{z\rho F}\frac{1}{sin\theta}\left(i_{a0} - i_s sin\theta\right)\end{aligned} \tag{34}$$

This can occur either because of the extremely high wear intensity or as a result of low passivation capability of the metal in the given environment or a combination of both.

According to the definition of wear-enhanced corrosion, the first and second terms in Eq. (34) represent the total corrosion rate during wear-corrosion, K_c, and corrosion-only rate, K_{co}, respectively, i.e.,

$$K_{c,sat,lim} = \frac{M}{z\rho F}\frac{i_{a0}}{sin\theta} \tag{35}$$

$$K_{co} = \frac{M}{z\rho F} i_s \tag{36}$$

Equation (35) shows that, under highly activated corrosion conditions, the total corrosion rate is considerably higher than pure corrosion rate (Eq. (14), or (36), because $i_{a0} \gg i_s \geq i_s^0$. Equations (34) and (35) also suggest that the wear-enhanced corrosion and total corrosion rate during combined wear and corrosion process are affected by the roughening of the wear surface: sharp abrasives (smaller θ) will increase the total corrosion rate.

According to Eqs. (4) and (13),

$$(1/x)^2 = \frac{4\tau^2(K_{wo} n v_x tan\theta)}{f_r} \propto K_{wo} \tag{37}$$

To get a sense about the general trend for the effect of wear intensity on wear-enhanced corrosion, the variations of $g(x)$ in Eq. (28) (Eq. (29)) and $m(x)$ in Eq. (32) (Eq. (33)) as a function of $(1/x)^2$ ($\sim K_{wo}$) at three (arbitrarily chosen) k values are calculated and shown in Fig. 6. At low wear intensity ($(1/x)^2 < 1$), wear-enhanced corrosion is determined by Eq. (29) which is represented by

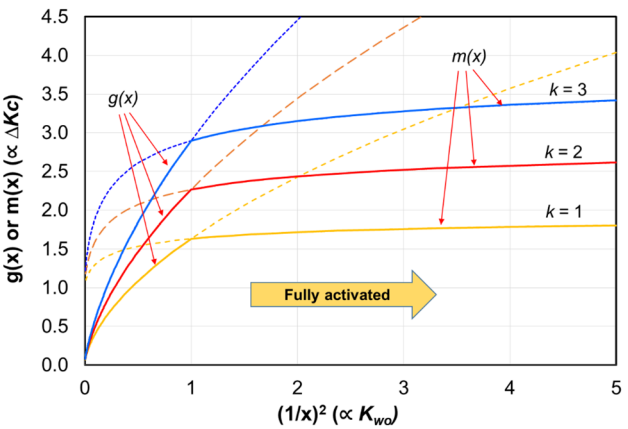

Fig. 6 The predicted general trend (solid lines) for the variation of wear-enhanced corrosion as a function of wear intensity. Wear-enhanced corrosion is represented by functions $g(x)$ in Eq. (29) and $m(x)$ in Eq. (33) for low and high wear intensity conditions, respectively. The abscissa, $(1/x)^2$, represents wear intensity, Eq. (37). (Both axes in the figure are dimensionless.)

the solid line portion of the function $g(x)$ in Fig. 6; ΔK_c increases rapidly with the increase in wear intensity. When the whole wear surface is fully activated (saturated activation), i.e., at $(1/x)^2 \geq 1$, the dependence of wear-enhanced corrosion is described by Eq. (32) which is represented by the function $m(x)$ in Fig. 6 (the solid lines portion). The wear-enhanced corrosion becomes much less sensitive to further increase in wear intensity.

3.2.3 Comparison with Published Experimental Data

Figure 7 replots some published experimental data adapted from [111] and [6] for the variation of wear-enhanced corrosion as a function of wear intensity. Figure 7a shows results from erosion-corrosion test for EN30B low alloy steel. Plotted in Fig. 7b are results for AISI D2 tool steel (60.5 HRC) tested under sliding abrasion-corrosion conditions. Slurries used in both tests were mixed from AFS50-70 silica sand and 3.5%NaCl solution. In Fig. 7c, data in Fig. 7a and b are combined and plotted in the same chart to show the relative severity of wear conditions in the two testing methods. It is apparent that the erosion-corrosion test is in the mild or low wear intensity regime; the wear-enhanced corrosion increases rapidly with the increase in wear intensity, Fig. 7a. On the other hand, under the sliding abrasion-corrosion test conditions, the wear surface reached saturated activation status at sliding velocities greater than 16 rpm. As a result, wear-enhanced corrosion rate increases very slowly with further increase in, or almost independent of, sliding speed/wear intensity, Fig. 7b & and c.

Using an array electrodes technique in a slurry pipe loop, Zeng et al. [83] experimentally measured the erosion-corrosion synergy of API X65 pipeline steel at different locations inside a 90° elbow. The slurry was a mixture of 1.2wt% silica sand (400–500 µm) and a CO_2-saturated complex solution simulating the formation water in an oil field. The slurry flow velocity was 4 m/s and the test was conducted at 60 °C. The testing results for erosion-enhanced corrosion, ΔK_c, as a function of erosion intensity, K_{wo}, are reproduced in Fig. 7d.

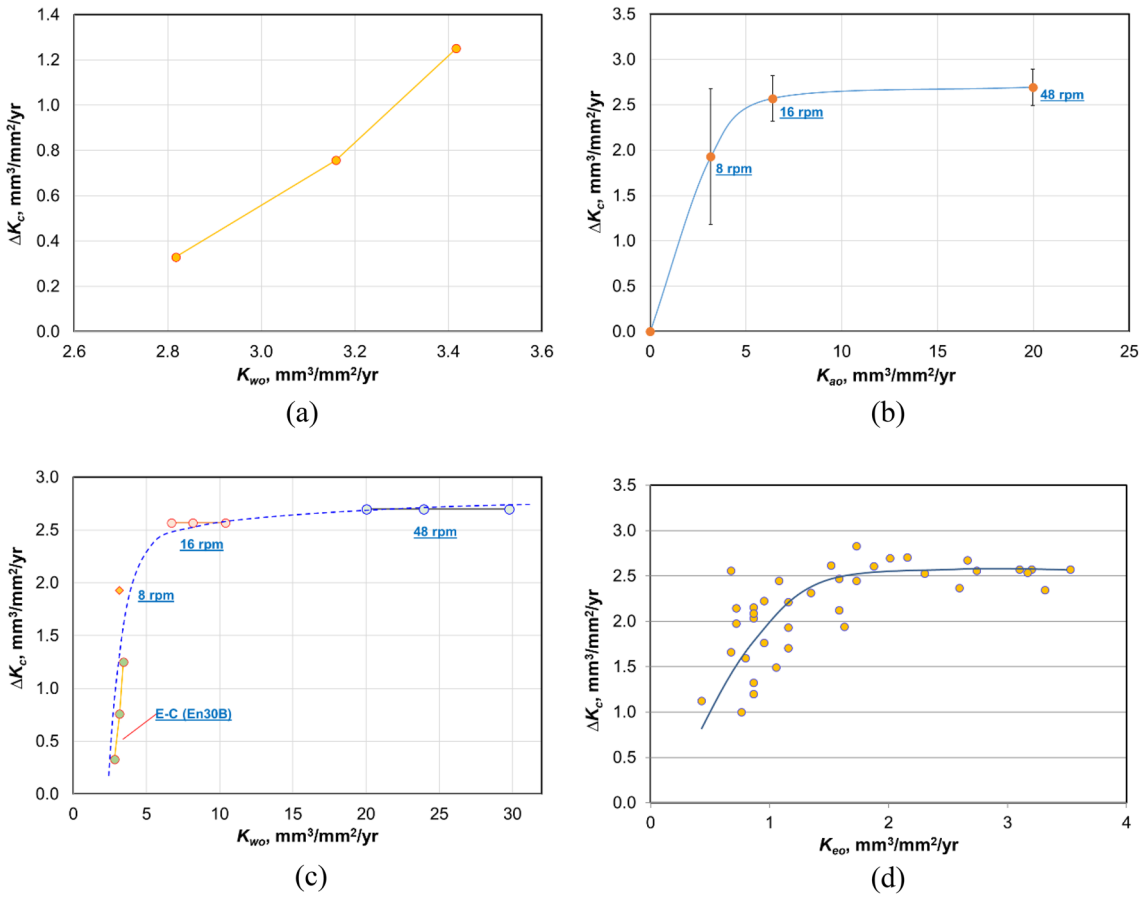

Fig. 7 Experimental data for relationship between wear-enhanced corrosion and wear intensity. **a** Data adapted from ref. [111] for EN30B low alloy steel under erosion-corrosion conditions in a 35wt% AFS 50–70 silica slurry in 3.5%NaCl solution; **b** AISI D2 tool steel under abrasion-corrosion conditions in 50wt% AFS 50–70 silica slurry in 3.5%NaCl solution [6]; **c** combined data from (**a**) and (**b**); and **d** low carbon steel pipe under erosion-corrosion conditions in a slurry pipe loop [83]

Again, a saturation phenomenon for wear-enhanced corrosion is observed with the increase in wear intensity.

The above results agree very well with the predicted trends in Fig. 6.

Using a rotating ring erosion tester, Lu et al. [20] studied the erosion-corrosion behavior of a 1045 steel in AFS50-70 silica sand/Edmonton tap water slurries at velocities (linear velocity at the rotating cylindrical specimen surface) from 4 m/s to 8 m/s. It was found that the wear-enhanced corrosion ΔK_c can be related to pure erosion rate K_{eo} by the following equation:

$$\frac{\Delta K_c}{K_{co}} = \lambda {K_{eo}}^{a+b-2} \tag{38}$$

where λ, a, and b are constants, K_{eo} is the pure erosion rate (mm/y), and $(a+b) \approx 2.8$. This empirical formula takes similar form to Eqs. (16) or (26). It should be pointed out that, although the velocities quoted in the study by Lu et al. [20] appear to be fairly high, the actual erosion intensity is expected to be low because erosion in a rotating ring tester is mostly at low impingement angles. Thus, the activation of the specimen surface due to mechanical erosion was most probably not saturated in those studies. Therefore, the wear-enhanced corrosion increases with pure erosion rate (to the power of 0.8), corresponding to the condition of $(1/x^2) < 1$ in Fig. 6.

On the other hand, in 1974, Postlethwaite et al. [112] studied the corrosion component of erosion-corrosion of a low carbon steel pipe carrying different types of ores in a pipe loop system. It was reported that there was no substantial effect of particle concentration and flow rate on the corrosion process during the erosion-corrosion attack in the potash slurry. The test conditions might have been in the severe erosion (high wear intensity) regime because dense slurries containing 24 vol% to 44 vol% of solids were used in the study.

3.3 Corrosion-Enhanced Wear

According to Eq. (6), corrosion-enhanced wear is a strong function of wear-only loss rate, K_{wo}. It also depends on the ratio of the thickness of corrosion-degraded layer, h_d, to the depth of wear penetration, h_w, i.e., h_d/h_w. As has been discussed in Sect. 2.1, mechanisms for the formation of corrosion-degraded layer are still very poorly understood and are likely different depending on the particular tribosystem. For example, in materials with heterogeneous microstructures such as in high chromium white cast irons and in tungsten carbide welding overlays, corrosion degradation will occur more rapidly in regions near the interface between the noble carbide particles and the adjacent metal matrix due to the galvanic corrosion effect. The "degraded layer" in such cases is non-uniform and tends to be much deeper than in materials with more uniform microstructures such as steels where the corrosion-degraded layer is expected to be more uniform over the wear surface. In deriving Eq. (6), detailed mechanisms on the degradation layer formation have been omitted and their effects on corrosion-enhanced wear are embedded in the parameters β and h_d. Thus, Eq. (6) is applicable for a broad range of wear-corrosion situations and provides a useful basis for deriving some general trends about the major factors affecting corrosion-enhanced wear and synergy in abrasion-corrosion or erosion-corrosion.

Based on Eq. (6) and the discussions to be made below, the possible trends for the variation of ΔK_w as a function of K_{wo} can be schematically depicted by Fig. 8a. The effect of wear intensity on ΔK_c, which has been discussed in Sect. 3.2 above (Fig. 6), is also included in Fig. 8a. From Fig. 8a and Eqs. (20, 21, 22, 23, 24), the effect of wear intensity on the various components of wear and corrosion rates can be constructed and are schematically presented in Fig. 8b. The values used in these figures are hypothetic and arbitrary and are for illustrations only. These postulated trends are further explained below.

(1) At the low wear intensity levels where the thickness of the corrosion-degraded layer developed on a given location of the wear surface between two successive wear events is greater than or equal to the wear penetration depth, i.e., when $h_d \geq h_w$, the mechanical wear occurs completely within the corrosion-degraded layer. This is outside the applicable conditions for Eq. (6) which is valid for $0 \leq h_d/h_w \leq 1$. According to the definition of the parameter β (Eq. (5)), the corrosion-enhanced wear under such conditions is proportional to the wear-only loss rate, K_{wo}, i.e.,

$$\Delta K_w = \beta K_{wo} \tag{39}$$

The corrosion-enhanced wear increases linearly with the increase in wear intensity when $h_d \geq h_w$, Fig. 8a.

(2) With the increase in wear intensity, the wear penetration depth exceeds the corrosion-degraded layer thickness, $h_w \geq h_d$, and the mechanical wear starts to involve both the corrosion-degraded layer and the material underneath that is not affected by corrosion. In this regime, the corrosion-enhanced wear (Eq. (6)) is a function of both the wear intensity, K_{wo}, and the term in the square bracket of Eq. (6), $\left[1 - \left(1 - \frac{h_d}{h_w}\right)^2\right]$. This term can be regarded as the enhancement factor for corrosion-enhanced wear. The "enhancement" effect of this term will become clear after the discussion in following paragraph.

The ratio h_d/h_w is an indirect/implicit function of wear intensity K_{wo}. The values of h_d and h_w may be affected in different manners depending on the way that wear intensity is changed. For example, if the increase in wear intensity is

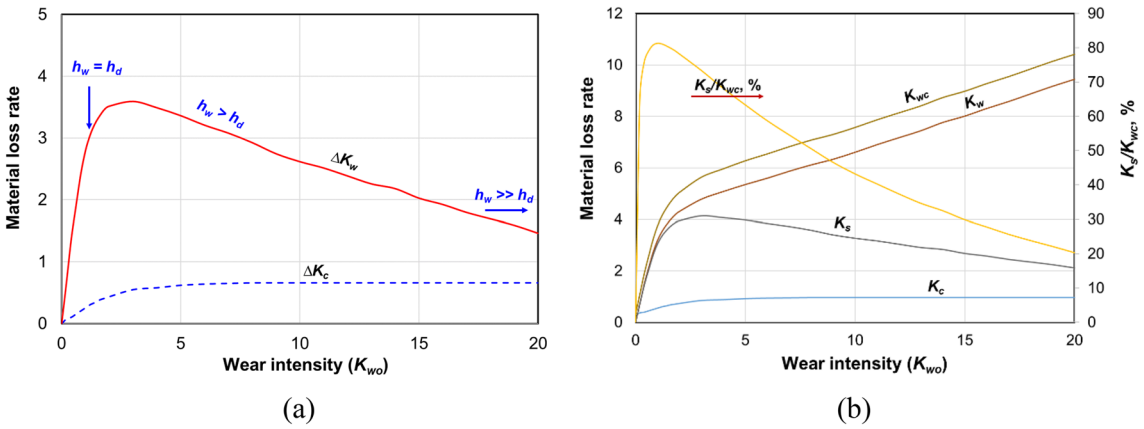

Fig. 8 Schematic diagrams showing the possible trends for the variation of various components of wear-corrosion synergy as a function of wear intensity, K_{wo}. These charts are based on qualitative discussions of the derived equations in the model. **a** Individual components of synergy; **b** Total wear and corrosion. (*Note* The figures are schematic and the values are arbitrary. Therefore, no units are used in the axes.)

a result of increased contact stress such as due to increased load in abrasion-corrosion, higher particle impingement velocity in erosion-corrosion, or due to wear by larger or sharper abrasive particles, then the wear penetration depth, h_w, will increase but the thickness of corrosion-degraded layer h_d will remain largely unchanged, as schematically indicated by Fig. 9a ($h_{w2} > h_{w1}$). In such conditions, the ratio h_d/h_w will decrease with the increase in wear intensity. On the other hand, if the increase in wear intensity is due to increased frequency of wear events, e.g., by higher solid concentration in the slurry (n) or higher motion velocity (v_x) of the abrasive particles relative to the wear surface or both, then the wear penetration depth does not change (i.e., h_w remains the same) but the thickness of corrosion-degraded layer, h_d, will decrease because the time for corrosion degradation between consecutive wear events at a given point of the wear surface (t_c, Eq. (13)) is reduced, Fig. 9b ($h_{d2} < h_{d1}$). There may also be situations where the increase in wear intensity is due to a combination of both increased contact stress and higher wear contact frequency. However, the ratio h_d/h_w will always decrease with the increase in wear intensity in any of these situations.

The variation of the enhancement factor for corrosion-enhanced wear in Eq. (6), $\left[1-\left(1-\frac{h_d}{h_w}\right)^2\right]$, as a function of the h_d/h_w ratio is plotted in Fig. 10 which shows that the enhancement factor decreases with the increase in wear intensity K_{wo} (decrease in h_d/h_w).

From the above discussions, the two parameters in Eq. (6), K_{wo} and the ratio h_d/h_w, have opposite effects on the corrosion-enhanced wear, ΔK_w. Depending on the actual conditions in a given tribosystem, corrosion-enhanced wear may either increase or decrease with increase in wear intensity after h_w becomes greater than h_d. However, it is expected that, at least at h_w values close to h_d, ΔK_w will increase with K_{wo} because a majority of mechanical wear will occur within the corrosion-degraded layer, although the rate of increase in ΔK_w with the increase of wear intensity will be reduced, i.e., the ΔK_w curve becomes bent down with the increase in wear intensity after $h_w > h_d$, as shown in Fig. 8a.

With further increase in wear intensity, the contribution of wear intensity K_{wo} will eventually become more dominant than the influence of the enhancement factor, Eq. (6) and Fig. 10. ΔK_w will reach a peak at some point

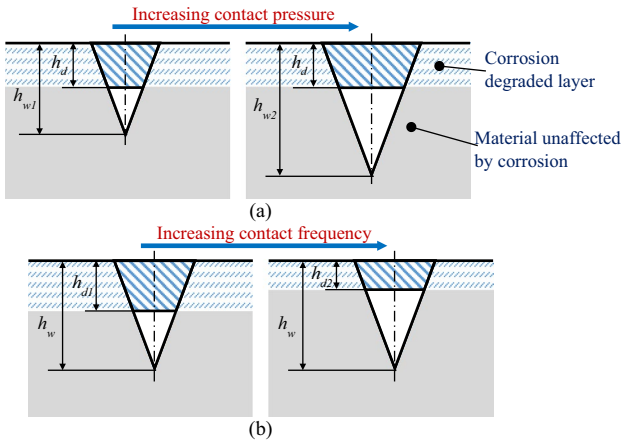

Fig. 9 Schematic diagrams showing the relative changes of wear penetration depth, h_w, and corrosion-degraded layer thickness, h_d, under different wear conditions where the increase in wear intensity, K_{wo}, is caused by different reasons: **a** increased contact stress between the abrasive particle and the wear surface such as by higher load and/or larger/sharper abrasive particles; **b** increased frequency of wear events at a given surface location such as by higher slurry concentration or higher relative sliding velocity of the abrasive particles over the wear surface

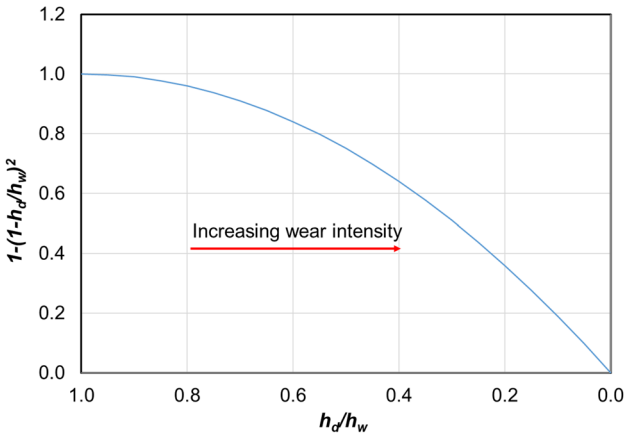

Fig. 10 Effect of the h_d/h_w ratio on the enhancement factor for corrosion-enhanced wear in Eq. (6), $\left[1-\left(1-\frac{h_d}{h_w}\right)^2\right]$

and eventually decrease with further increase in wear intensity, Fig. 8a. This trend can be further confirmed by considering the following scenario.

(3) When $h_w >> h_d$ (i.e., $h_d/h_w \rightarrow 0$), which can be a result of very high wear intensity (high penetration depth and/or high frequency of wear events) or very low corrosion severity (high corrosion resistance or low corrosivity) or a combination of both, according to Eq. (6), the corrosion-enhanced wear diminishes, $\Delta K_w \rightarrow 0$,

$$\Delta K_w \approx 0 \tag{40}$$

This scenario (3) is a limiting situation associated with high relative wear intensity. In such conditions, corrosion-degraded layer on the wear surface, and thus corrosion-enhanced wear, becomes negligible. It should be pointed out that, although corrosion-enhanced wear is now minimal, wear-enhanced corrosion and thus the total synergistic effect may still be significant because fresh/activated metal surface is constantly created by the mechanical wear actions (ΔK_c in Fig. 8a). The synergy will be dominated by wear-enhanced corrosion. The significance of the wear-enhanced corrosion will depend on the corrosion properties of the material in the given environment (corrosion media, material response to plastic deformation, repassivation, etc.).

After the variations of ΔK_w and ΔK_c are established in Fig. 8a, the variations of material loss rate due to corrosion (K_c) and mechanical wear (K_w), the total synergy (K_s), and the total wear-corrosion loss rate (K_{wc}) can be easily constructed as shown in Fig. 8b by applying the relationships in Eqs. (20, 21, 22, 23, 24). The total corrosion rate (K_c) is the sum of pure corrosion (K_{co}) and wear-enhanced corrosion (ΔK_c), Eq. (24). Since K_{co} is the corrosion rate in the absence of wear and is a constant unaffected by wear intensity, K_c shows the same trend as that for ΔK_c, shifting up by a constant value of K_{co}. On the other hand, the total material loss rate due to mechanical wear (K_w) is the sum of pure wear (K_{wo}) and corrosion-enhanced wear (ΔK_w) and is thus a linear function of K_{wo}. As discussed above, K_w will eventually become a linear function of the wear intensity (K_{wo}) because corrosion-enhanced wear (ΔK_w) becomes negligible at very high wear intensity levels, showing a continuous increase at high wear intensity values, Fig. 8b.

3.3.1 Comparison with Published Data in the Literature on Corrosion-Enhanced Wear

In the erosion-corrosion study by Lu et al. [20] on a 1045 steel, the corrosion-enhanced erosion was attributed to surface softening under anodic current flow (the chemo-mechanical effect) and the following expression was found to properly describe the experimental results:

$$\frac{\Delta K_e}{K_{eo}} = Z\ln\frac{K_c}{K_{eo}} + D \tag{41}$$

where Z and D are experimental constants. ΔK_e, K_{eo}, and K_c are material loss rates for corrosion-enhanced erosion, pure erosion, and total corrosion, respectively.

Similar to Eq. (6), the Eq. (41) identifies two major factors affecting corrosion-enhanced wear (erosion), i.e., the pure erosion rate (the wear intensity), K_{eo}, and the ratio between total corrosion and pure erosion, K_c/K_{eo}. This equation predicts that corrosion-enhanced erosion (wear) increases with wear intensity (the pure erosion rate K_{eo}) and the ratio K_c/K_{eo}. According to the discussion preceding this sub-section, the ratio K_c/K_{eo} will tend to decrease with the increase in wear intensity (K_{eo}). Thus, the general trends predicted by the model presented in the current paper agree with Eq. (41) which was derived from experimental data [20].

The ratio K_c/K_{eo} in Eq. (41) can be directly related to the ratio (h_d/h_w) in Eq. (6). Both represent the relative intensity of damage caused by corrosion to that by mechanical wear. In homogeneous materials or if the corrosion-degraded layer responsible for the accelerated wear loss is homogeneous, the thickness of corrosion-degraded layer, h_d, may be proportional to or predominantly determined by the total corrosion intensity, K_c. However, when localized corrosion is the dominant mechanism for corrosion-enhanced wear such as preferential corrosion along phase boundaries in Cr white cast irons or other heterogeneous/composite microstructures, the total corrosion rate may not be a reliable indicator for the degree of corrosion-enhanced wear. Under such conditions, Eq. (41) may not be applicable. In comparison, the parameter h_d introduced in our model has more clear physical meanings and should be more adequate for studying the

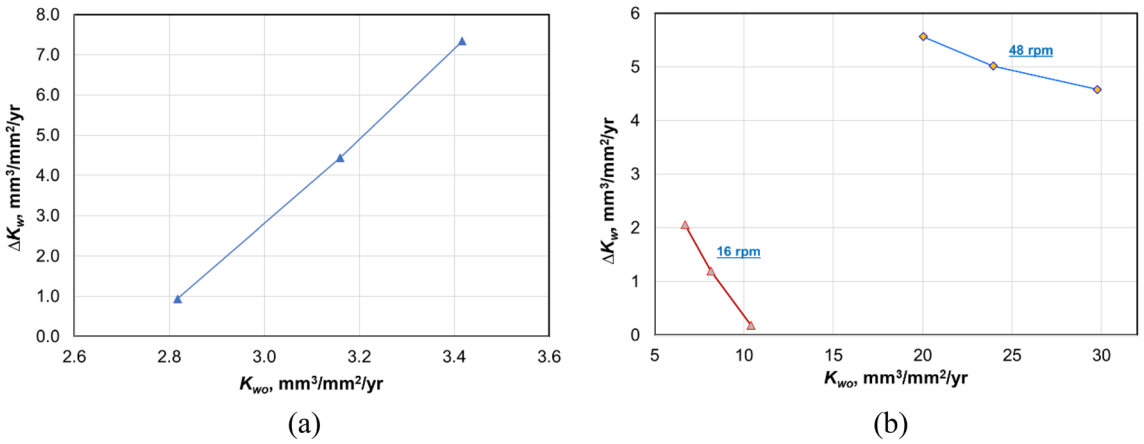

Fig. 11 Experimental data for corrosion-enhanced wear as a function of wear intensity in **a** erosion-corrosion for EN30B low alloy steel [111]; and **b** abrasion-corrosion for D2 tool steel [6]

synergistic effect in different tribosystems including both homogeneous and heterogeneous microstructures.

In Fig. 11, experimental results on the variation of corrosion-enhanced wear as a function of wear intensity obtained from erosion-corrosion test of En30B steel [111] and abrasion-corrosion study of AISI D2 tool steel [6] are reproduced. These two sets of data were obtained in the same studies corresponding to the wear-enhanced corrosion data in Fig. 7a and Fig. 7b, respectively. As discussed in Sect. 3.2 (Fig. 7c), the erosion-corrosion test conditions were very mild (Fig. 7a, Fig. 11a). It is reasonable to expect the wear regime in these tests to fall in the range of $h_d \geq h_w$ as depicted in Fig. 8. Therefore, corrosion-enhanced wear (erosion) rate increases with the increase in wear intensity at the low wear intensity region. On the other hand, the abrasion-corrosion test was conducted under high wear intensity conditions (Fig. 7c) and probably fall in the region where $h_w > h_d$ in Fig. 8. The corrosion-enhanced wear decreased with the increase in wear intensity for tests at the sliding speed of 16 rpm and 48 rpm, respectively, Fig. 11b, which agrees with the general (decreasing) trend as illustrated in Fig. 8a for $h_w > h_d$, although the results from the two different sliding speeds do not fall on the same line.

Elemuren et al. [28] experimentally studied the erosion-corrosion of AISI 1018 steel 90° elbow using a continuous slurry flow loop in saturated potash brine and sand slurry containing 10, 20, and 30 wt% silica particles at slurry flow velocities of 2.5 and 4.0 m/s. It was found that the percentage contribution of synergistic effect is considerably higher at the lower slurry velocity of 2.5 m/s (49%) than at 4.0 m/s (12%). Due to the high concentration of solids in the slurry, it is reasonable to expect that the erosion conditions fall in the $h_w > h_d$ regime, i.e., in the high wear intensity region beyond the peak for K_s or K_s/K_{wc} curve in Fig. 8b. Therefore, the relative synergy contribution decreases with the increase in slurry velocity which causes more severe wear (higher wear intensity).

Marsden [39] studied the erosion-corrosion synergism of three steels, including A514 (284 HV), 316 SS, and a commercial AR500 steel (REM 500), using a flow-through slurry erosion test apparatus in a slurry containing 0.06 M Na_2SO_4 and 2% solids (AFS50-70) in tap water. The impeller velocities are 5.8 and 15.6 m/s and the tests were conducted at 26 and 60 °C, respectively. The results of various material loss rate obtained from this study are adapted and replotted in Fig. 12a as a function of wear intensity (pure erosion rate, K_{eo}). Interestingly, results for the different steels under the different test conditions all fell on the same trend lines. The corrosion-enhanced erosion, ΔK_e, increases monotonously with wear intensity. In this study, a 2wt% AFS50-70 silica dilute slurry was used. It is reasonable to assume that the erosion conditions are mild and there was sufficient time to form corrosion-degraded layer in the wear surface that is thicker than wear penetration depth, h_w. This can be confirmed by the results for the total corrosion rate, K_c, in Fig. 12a which is seen to increase with the wear intensity. Discussions in Sect. 3.2 showed that such behavior is associated with the situation where the erosion conditions are mild and likely in the $h_d > h_w$ regime as illustrated in Fig. 8. Therefore, the corrosion-enhanced wear increases with the increase in wear intensity.

The results reported in [83] for the various synergy components measured over the various locations inside the 90° X65 steel elbow have been extracted and are replotted in Fig. 12b against the erosion intensity, K_{eo}. For completeness, the ΔK_c data already presented in Fig. 7d are also included in the figure. Despite the different erosion conditions (e.g., impingement angle and actual slurry velocity) at the various locations inside the elbow and some data scatter at the low erosion intensity, some general trends are apparent. There is

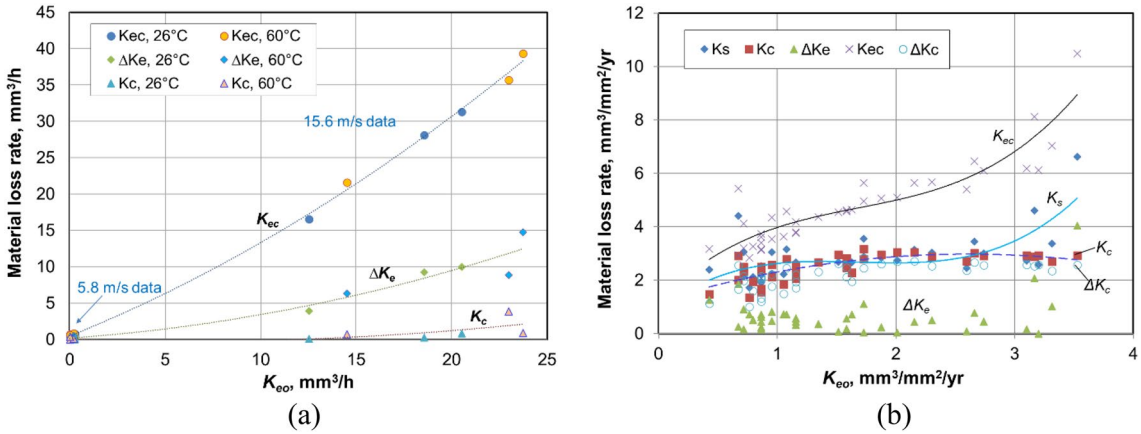

Fig. 12 Re-plots of erosion-corrosion experimental data extracted from **a** ref. [39] for three different steels tested at different slurry velocities and temperatures and **b** ref. [83]. The original results from [39] in (**a**) were not converted to thickness change rates ($mm^3/mm^3/yr$) because wear was not uniform over the whole test specimen surface [39]

significant erosion-enhanced corrosion (ΔK_c). ΔK_c increases slightly with the increase in erosion intensity but appears to reach some steady level at K_{eo} values greater than about 1.5 $mm^3/mm^2/yr$. Erosion-enhanced corrosion dominates the total synergy (K_s) at K_{eo} values below about 3 $mm^3/mm^2/yr$ above which the corrosion-enhanced erosion (ΔK_e) becomes more dominant. These trends generally agree with those illustrated in Fig. 8 within the $h_d > h_w$ erosion-corrosion regime for low/mild relative wear intensity situations; in such regime, corrosion-enhanced wear, total synergy, and total wear-corrosion loss rates all increase with the increase in wear intensity. These observations are in line with the very low solid concentration in the slurry (1.2 wt%) and the relatively low flow velocity (4 m/s) used in this study.

3.4 Overall Comments

According to the above comparison between published data obtained from a range of experimental conditions and predictions of the proposed model on wear-enhanced corrosion (Fig. 7 vs Fig. 6 in Sect. 3.2.1) and on corrosion-enhanced wear (Eqs. (41) vs (6) and Figs. 11, 12 vs 8 in Sect. 3.3.1), reasonably good agreement is observed in terms of the general trends. As is the case for most tribology studies, it is impractical to expect to reliably and quantitatively predict tribological behavior of a tribosystem based on first principles. However, the good qualitative agreement between experimental observations and the model prediction suggests that the main concepts used in developing the model are reasonable and can be applied to analyze synergistic effects in wear-corrosion by hard particles. In particular, the model shows that the relative severity between corrosion and wear can change the relative contributions of the two components of synergy, i.e., wear-enhanced corrosion and corrosion-enhanced wear, for the same material-environment system. For example, when mechanical wear intensity is low, corrosion and wear-enhanced corrosion would dominate the synergy. But under severe wear conditions, the relative contribution of corrosion (pure corrosion and wear-enhanced corrosion) will become less important.

Although the model has been developed mostly based on homogeneous microstructures, the concepts and derived conclusions can also be usefully applied to analyze/interpret results obtained from materials with inhomogeneous/heterogeneous microstructures. Among the various corrosion-enhanced wear mechanisms proposed so far as summarized in the Introduction, the corrosion-degraded material can be regarded as a relatively uniform layer with a thickness of h_d if the process involves dissolution of work hardening layer (Mechanism (2.1)), the chemo-mechanical softening effect due to anodic corrosion current (Mechanism (2.3)), or the lowering of fatigue strength in the corrosive environment (Mechanism (2.5)). On the other hand, if the corrosion-enhanced wear is due to preferential corrosion in heterogeneous microstructures or along the grain boundaries (Mechanism (2.2)) or localized corrosion attacks (Mechanism (2.4)), then the corrosion-degraded material will include both the directly damaged material and material in the surrounding region that has been weakened by the localized attacks; these affected materials can be more easily removed by the action of mechanical wear. In these non-uniform corrosion-degradation cases, an equivalent depth of corrosion-degraded material layer can be defined by dividing the volume of weakened material involved in the wear process by the apparent area of the wear surface. In some other cases, this thickness may also possibly refer to the density of defects (degree of degradation) accumulated in the near surface region.

In terms of wear-enhanced corrosion, the model is explicitly based on the Mechanism (1.1) in the Introduction, i.e., it

is a result of exposing fresh/active metal surface due to wear. However, the roughening effect as proposed in the Mechanism (1.3) is directly predicted in the derived Eq. (26) in Sect. 3.2.1 and Eq. (35) in Sect. 3.2.2. The other mechanisms for wear-enhanced corrosion listed in the Introduction, i.e., Mechanism (1.2) (accelerated mass transport), Mechanism (1.4) (higher energy more active metal surface), and Mechanism (1.5) (increased localized corrosion due to acidification), can be indirectly taken into account by incorporating their effects on the corrosion dynamics parameters such as i_{a0}, i_a, i_s, and τ.

An important concept introduced in the model developed in this paper is that corrosion-enhanced wear is due to the formation of a corrosion-degraded layer in the wear surface. This concept and the model can be developed further to include antagonistic abrasion-corrosion events. Antagonism may be observed when the wear surface is protected by the formation of tribo-films [40, 41] or, as mentioned in [44, 45], by the shot peening effect due to the impact of the metal surface by high velocity erodent particles. In those cases, the corrosion-degradation layer in the previous discussions should be substituted by wear protective tribo-layer where the parameter β in Eq. (5) will have negative values.

From the material selection perspective, corrosion resistance is important for relatively low wear intensity applications but wear resistance should be the major consideration under severe wear working conditions. As an example, as has been argued by the authors in ref. [111], chromium white irons containing higher Cr% (e.g., ASTM A532 IIIA or 27%Cr) may be advantageous for wet components of slurry pumps when wear/erosion is not very severe (such as when handling fine sand, low solid concentration slurry, and/or in high corrosion medium). However, when the erosion conditions are severe such as when handling dense slurries and/or when large particle abrasives are being processed, the more wear resistant lower chromium grades of chromium white irons (e.g., ASTM A532 IIB or 15%Cr–Mo) would be more beneficial. In the erosion-corrosion study of a group of high chromium white irons using a slurry pot tester, Islam et al. [113] showed that, while the hyper-eutectic chromium white iron had high erosion resistance under pure erosion conditions, it suffered very severe synergistic loss in erosion-corrosion conditions due to corrosion-enhanced erosion. This is attributed to the low Cr concentration remaining in the matrix after the formation of the primary and eutectic carbides. During the erosion-corrosion test, rapid and deep preferential corrosion occurred in the matrix along phase boundaries between the carbide and the matrix (high h_d), significantly weakening the support of the carbide by the matrix. Thus, hyper-chromes are not suited for wear applications where corrosion is expected.

Similarly, the concepts and relationships derived in the model can be applied to help more properly interpret and translate lab wear-corrosion testing results for predicting performance in potential applications by taking into account differences in working conditions (relative severity of corrosion and mechanical wear) between lab testing and the application.

4 Summary

A model for wear-corrosion during hard particle wear has been presented. The model describes major parameters affecting the two components of synergy, i.e., wear-enhanced corrosion and corrosion-enhanced wear. Wear is calculated based on the grooving (micro-cutting and micro-ploughing) mechanism by the sliding of a conical shaped hard particle over the wear surface. For hard particles having a known semi-tip angle of θ, the wear rate is defined by the penetration depth, h_w, the number of particles, and the velocity of sliding over the wear surface. Wear-enhanced corrosion is assumed to be due to the generation of fresh (depassivated) metal surface by wear. On the other hand, corrosion-enhanced wear is assumed to be mainly caused by the formation of a weakened/degraded layer near the wear surface under the influence of corrosion. Under the same wear conditions, material loss rate within this corrosion-degraded layer is higher than in the original material that has not been affected by corrosion. The mechanisms for the formation of such a layer and its natures/characteristics are not defined in this work and need further investigation. It will vary depending on conditions in each individual tribosystem.

According to the model, the relative thickness of the corrosion-degraded layer (h_d) to the depth of hard particle penetration (h_w), or the ratio h_d/h_w, is an important parameter in determining the synergistic effect. The corrosion-degraded layer is related to the severity of corrosion damage, while the depth of hard particle penetration signifies the intensity of mechanical wear (i.e., the wear-only loss rate). At low relative wear intensity conditions where $h_d > h_w$, wear occurs completely or primarily within the corrosion-degraded volume of material and high corrosion-enhanced wear is expected. When the wear penetration depth exceeds the corrosion-degraded layer, $h_w > h_d$, material removal occurs in both the corrosion-degraded volume and the material unaffected by corrosion. In this regime, the relative contribution of corrosion-enhanced wear to total material loss decreases with increase in the wear intensity. In severe relative wear conditions where $h_w >> h_d$, the contribution of corrosion-enhanced wear to synergy diminishes and the material loss is dominated by mechanical wear.

Since wear-enhanced corrosion is proportional to the fresh metal surface area generated by mechanical wear, it

is mainly controlled by the intensity of wear. The model predicts that wear-enhanced corrosion increases with wear intensity at low wear intensity levels but will level off and reach some steady value when the wear intensity exceeds certain level. This leveling off phenomenon is related to the fact that when the wear intensity is high enough, the whole wear surface is constantly depassivated by the mechanical wear and the corrosion rate is saturated.

Reasonably good qualitative agreement has been observed between the model predictions and experimental erosion-corrosion and abrasion-corrosion testing data from the published literature.

Appendixes

Appendix A Calculation of Repassivation Time Interval, t_c

The repassivation time interval, t_c, can be estimated as follows. Consider a site on the wear surface that is activated by a wear event at time $t=0$. Following the wear event, the surface starts to repassivate until the next wear event occurs on the same site. At any time, there are an average of n wear events occurring on a unit apparent area of the wear surface, each creating a projected activated area of A_a within unit time. Thus, the total projected area, $A_{a,t}$, on unit apparent surface area within the time interval between 0 and t_c is equal to

$$A_{a,t} = nA_a v_x t_c \tag{42}$$

Assume that all the wear events occur randomly, and are distributed uniformly, over the wear surface. Within a certain period of time (t_c), each location of the whole apparent area of the wear surface will have been activated once by an individual wear event. At time $t > t_c$, statistically, a new wear event will repeat at the same previously activated given location of interest, creating the next activated surface area and terminating the previous repassivation process. This condition corresponds to $A_{a,t}=1$ and the time required for achieving this status is the repassivation time, t_c. Thus, from Eq. (42), t_c can be calculated by

$$t_c = \frac{1}{nA_a v_x} = \frac{1}{2nv_x h_w tan\theta} \tag{43}$$

Appendix B Effect of Wear Intensity on Wear-Enhanced Corrosion for Metals with Exponential Transient Current Decaying Behavior

This Appendix considers the wear-enhanced corrosion for the special case where the transient corrosion current, i_a, on the freshly exposed metal surface during wear follows the exponential decay behavior described by Eq. (27).

Substituting Eqs. (27) into (16), the wear-enhanced corrosion, ΔK_c, is obtained by

$$\begin{aligned}\Delta K_c &= \frac{M}{z\rho F}\left(\frac{1}{t_c sin\theta}\right)\left\{\frac{\tau}{t_c}\left(i_{a0}-i_s\right)\left[1-\exp\left(-\frac{t_c}{\tau}\right)\right]+(1-sin\theta)i_s\right\} \\ &= \frac{M}{z\rho F}2\left(\frac{K_{wo}nv_x}{f_r sin\theta cos\theta}\right)^{\frac{1}{2}}\left\{\frac{\tau}{t_c}\left(i_{a0}-i_s\right)\left[1-\exp\left(-\frac{t_c}{\tau}\right)\right]+(1-sin\theta)i_s\right\}\end{aligned} \tag{44}$$

In Sect. 2.4.1, it was pointed out that the equations for K_c or ΔK_c (Eqs. (10) and (16)) are applicable when the condition in Eq. (11) is met. By applying eq. (43), the condition Eq. (11) can be expressed by

$$t_c = \frac{1}{2nv_x h_w tan\theta} > 1 \tag{45}$$

Thus, Eq. (44) is valid only at lower levels of wear intensity, K_{wo}.

Under high wear intensity conditions where $t_c \le 1$, the wear surface activation is saturated, i.e., further increase in wear intensity will not significantly create more fresh metal surface areas. The wear-enhanced corrosion in such conditions, $\Delta K_{c,sat}$, can be expressed by the following equation by substituting Eq. (27) into Eq. (18):

$$\Delta K_{c,sat} = \frac{M}{z\rho F}\frac{1}{sin\theta}\left\{\frac{\tau}{t_c}(i_{a0}-i_s)[1-\exp(-\frac{t_c}{\tau})]+i_s(1-sin\theta)\right\} \tag{46}$$

When wear is very severe and/or if the metal is difficult to repassivate (with high characteristic repassivation time τ), the value t_c/τ becomes very small ($t_c << \tau$),

$$\lim_{(t_c/\tau)\to 0}\left\{\frac{\tau}{t_c}[1-\exp(-\frac{t_c}{\tau})]\right\} = 1$$

and Eq. (46) is reduced to

$$\begin{aligned}\Delta K_{c,sat,lim} &= \frac{M}{z\rho F}\frac{1}{sin\theta}\left[(i_{a0}-i_s)+i_s(1-sin\theta)\right] \\ &= \frac{M}{z\rho F}\frac{1}{sin\theta}\left(i_{a0}-i_s sin\theta\right)\end{aligned} \tag{47}$$

Let

$$x = \frac{t_c}{\tau} \tag{48}$$

and

$$k = \frac{\left(i_{a0} - i_s\right)}{(1 - sin\theta)i_s} \tag{49}$$

Equation (44) can be expressed as

$$\begin{aligned}\Delta K_c &= \frac{M}{z\rho F}\left(\frac{1}{\tau sin\theta}\right)\frac{1}{x}\left\{\frac{1}{x}\left(i_{a0} - i_s\right)\left[1 - \exp(-x)\right] + i_s(1 - sin\theta)\right\} \\ &= \frac{M}{z\rho F}\left[\frac{(1-sin\theta)i_s}{\tau sin\theta}\right]\frac{1}{x}\left\{\frac{1}{x}k\left[1 - \exp(-x)\right] + 1\right\} \\ &= \frac{M}{z\rho F}\left[\frac{(1-sin\theta)i_s}{\tau sin\theta}\right]g(x)\end{aligned} \tag{50}$$

where

$$g(x) = \frac{1}{x}\left\{\frac{1}{x}k\left[1 - \exp(-x)\right] + 1\right\} \tag{51}$$

Similarly, Eq. (46) can be expressed in terms of x and k in Eq. (52):

$$\begin{aligned}\Delta K_{c,sat} &= \frac{M}{z\rho F}\frac{i_s(1-sin\theta)}{sin\theta}\left\{\frac{\tau}{t_c}\frac{(i_{a0}-i_s)}{i_s(1-sin\theta)}[1 - \exp(-\frac{t_c}{\tau})] + 1\right\} \\ &= \frac{M}{z\rho F}\frac{i_s(1-sin\theta)}{sin\theta}\left\{\frac{1}{x}k[1 - \exp(-x)] + 1\right\} \\ &= \frac{M}{z\rho F}\frac{i_s(1-sin\theta)}{sin\theta}m(x)\end{aligned} \tag{52}$$

where

$$m(x) = \left\{\frac{1}{x}k[1 - \exp(-x)] + 1\right\} \tag{53}$$

Author Contributions All authors contributed to the concept development in the mathematical modeling and the design of the study. The first draft of the manuscript was written by JJ and all authors commented on previous versions of the manuscript. All authors read and approved the final manuscript.

Funding Open Access funding provided by National Research Council Canada.

Data Availability Data used in this paper are available for sharing.

Declarations

Competing interests Jiaren (Jimmy) Jiang is a member of the Senior Advisory Editorial Board of the Journal of Bio- & Tribo-Corrosion, while Margaret M. Stack is the Editor-in-Chief of this journal.

Ethical Approval Not applicable.

References

1. Dunn D (1985) Metal removal mechanisms comprising wear in mineral processing, K.C. Ludema (Ed.), Proc. Int. Conf. on Wear of Materials, April 14–18, 1985, Vancouver, BC, Canada, pp.501–508.
2. Barker K, Ball A (1989) Synergistic abrasive-corrosive wear of chromium containing steels. Br Corros J 24:222–228
3. Noel R, Ball A (1983) On the synergistic effects of abrasion and corrosion during wear. Wear 87:351–361
4. Batchelor A, Stachowiak G (1988) Predicting synergism between corrosion and abrasive wear. Wear 123:281–291
5. Kotlyar D, Pitt C, Wadsworth M (1988) Simultaneous corrosion and abrasion measurements under grinding conditions. Corrosion 44:221–228
6. Jiang Jiaren, Yao Baisheng, Xie Yongsong (2021) The effect of test conditions on sliding abrasion-corrosion synergy of D2 tool steel in a salt slurry. Wear 477:203843
7. Wang S-H, Jiang J, Stack MM (2015) Methodology development for investigation of slurry abrasion corrosion by integrating an electrochemical cell to a miller tester. J Bio- Tribo-Corros 1:1–9
8. Ji J-L, Tang J-L (1990) Wear-corrosion behavior of cast-in composite materials reinforced by WC particles. Wear 138:23–32
9. Wieczorek AN, Wójcicki M (2021) Synergism of the binary wear process of machinery elements used for gaining energy raw materials. Energies 14:1981
10. De Souza V, Neville A (2003) Corrosion and erosion damage mechanisms during erosion–corrosion of WC–Co–Cr cermet coatings. Wear 255:146–156
11. Meng H, Hu X, Neville A (2007) A systematic erosion–corrosion study of two stainless steels in marine conditions via experimental design. Wear 263:355–362
12. Neville A, Reyes M, Xu H (2002) Examining corrosion effects and corrosion/erosion interactions on metallic materials in aqueous slurries. Tribol Int 35:643–650
13. Shrestha S, Hodgkiess T, Neville A (2005) Erosion–corrosion behaviour of high-velocity oxy-fuel Ni–Cr–Mo–Si–B coatings under high-velocity seawater jet impingement. Wear 259:208–218
14. Souza V, Neville A (2005) Corrosion and synergy in a WC Co Cr HVOF thermal spray coating – understanding their role in erosion–corrosion degradation. Wear 259:171–180
15. Wood RJ (2006) Erosion–corrosion interactions and their effect on marine and offshore materials. Wear 261:1012–1023
16. Madsen BW (1988) Measurement of erosion-corrosion synergism with a slurry wear test apparatus. Wear 123:127–142
17. Neville A, Hodgkiess T, Dallas J (1995) A study of the erosion-corrosion behaviour of engineering steels for marine pumping applications. Wear 186:497–507
18. Neville A, Hodgkiess T, Xu H (1999) An electrochemical and microstructural assessment of erosion–corrosion of cast iron. Wear 233:523–534
19. Hodgkiess T, Neville A, Shrestha S (1999) Electrochemical and mechanical interactions during erosion–corrosion of a high-velocity oxy-fuel coating and a stainless steel. Wear 233:623–634
20. Lu BT, Lu JF, Luo JL (2011) Erosion–corrosion of carbon steel in simulated tailing slurries. Corros Sci 53:1000–1008

21. Rajahram SS, Harvey TJ, Wood RJK (2009) Erosion-corrosion resistance of engineering materials in various test conditions. Wear 267:244–254
22. Burstein GT, Sasaki K (2000) Effect of impact angle on the slurry erosion-corrosion of 304L stainless steel. Wear 240:80–94
23. Lu BT, Luo JL (2006) Synergism of electrochemical and mechanical factors in erosion-corrosion. J Phys Chem B 110:4217–4231
24. Bateni MR, Szpunar JA, Wang X, Li DY (2006) Wear and corrosion wear of medium carbon steel and 304 stainless steel. Wear 260:116–122
25. Guo HX, Lu BT, Luo JL (2005) Interaction of mechanical and electrochemical factors in erosion-corrosion of carbon steel. Electrochim Acta 51:315–323
26. Postlethwaite J, Dobbin MH, Bergevin K (1986) The role of oxygen mass transfer in the erosion-corrosion of slurry pipelines. Corrosion 42:514–521
27. Abedini M, Ghasemi HM (2014) Synergistic erosion-corrosion behavior of Al-brass alloy at various impingement angles. Wear 319:49–55
28. Elemuren R, Evitts R, Oguocha I, Kennell G, Gerspacher R, Odeshi A (2018) Slurry erosion- corrosion of 90° AISI 1018 steel elbows in saturated potash brine containing abrasive silica particles. Wear 410:149–155
29. Souza VAD, Neville A (2007) Aspects of microstructure on the synergy and overall material loss of thermal spray coatings in erosion–corrosion environments. Wear 263:339–348
30. Hussain EAM, Robinson MJ (2007) Erosion-corrosion of 2205 duplex stainless steel in flowing seawater containing sand particles. Corros Sci 49:1737–1744
31. Barik RC, Wharton JA, Wood RJK, Stokes KR (2009) Electro-mechanical interactions during erosion-corrosion. Wear 267:1900–1908
32. Neville A, Reyes M, Hodgkiess T, Gledhill A (2000) Mechanisms of wear on a Co-base alloy in liquid–solid slurries. Wear 238:138–150
33. Neville A, Hodgkiess T (1999) Characterisation of high-grade alloy behaviour in severe erosion–corrosion conditions. Wear 233–235:596–607
34. Neville A, Reza F, Chiovelli S, Revega T (2005) Erosion-corrosion behavior of WC based MMCs in liquid-solid slurries. Wear 259:181–195
35. Jiang Jiaren, Yongsong Xie Md, Aminul Islam MM, Stack, (2017) The effect of dissolved oxygen in slurry on erosion–corrosion of En30B steel. J Bio-Tribo Corros. 3(3):45
36. Moine M, Mary N, Normand B, Peguet L, Gaugain A, Evin HN (2012) Tribo-electrochemical behavior of ferrite and ferrite–martensite stainless steels in chloride and sulfate media. Wear 292–293:41–48
37. Aminul Islam Md, Jiaren (Jimmy) Jiang, Yongsong Xie, Petr Fiala, (2017) Investigation of erosion-corrosion behavior of (WTi)C based weld overlays. Wear 390–391:155–165
38. Malka R, Nešić S, Gulino DA (2007) Erosion-corrosion and synergistic effects in disturbed liquid-particle flow. Wear 262:791–799
39. Marsden BW (1988) Measurement of erosion-corrosion synergism with a slurry wear test apparatus. Wear 123:127–142
40. Yueting Liu JMC, Mol G.C.A.M. Janssen (2015) Corrosion reduces wet abrasive wear of structural steel. Scripta Mater 107:92–95
41. Sinnett-Jones PE, Wharton JA, Wood RJK (2005) Micro-abrasion–corrosion of a CoCrMo alloy in simulated artificial hip joint environments. Wear 259:898–909
42. Xu J, Zhuo C, Tao J, Jiang S, Liu L (2009) Improving the corrosion wear resistance of AISI 316L stainless steels by particulate reinforced Ni matrix composite alloying layer. J Phys D 42:1–12
43. Rajahram SS, Harvey TJ, Wood RJK (2011) Electrochemical investigation of erosion–corrosion using a slurry pot erosion tester. Tribol Int 44:232–240
44. Wood RJK, Hutton SP (1990) The synergistic effect of erosion and corrosion: trends in published results. Wear 140:387–394
45. Wood RJK (1992) Erosion-corrosion synergism for muIti-phase flowline materials. La Houille Blanche 78:605–610. https://doi.org/10.1051/lhb/1992065
46. Postlethwaite J, Lotz U (1988) Mass transfer at erosion-corrosion roughened surfaces. Can J Chem Eng 66:75–78
47. Clark HM, Hartwich RB (2001) A re-examination of the 'particle size' effect in slurry erosion. Wear 248:147–161
48. Harvey TJ, Wharton JA, Wood RJK (2007) Development of a synergy model for erosion–corrosion of carbon steel in a slurry pot. Tribology 1:33–47
49. Postlethwaite J, Holdner DN (1975) Wall mass transfer in horizontal slurry pipelines. Can J Chem Eng 53:31–35
50. Postlethwaite J, Holdner DN (1976) Wall mass transfer in vertical and horizontal slurry pipelines. Can J Chem Eng 54:255–258
51. Burstein GT, Sasaki K (2001) Detecting electrochemical transients generated by erosion–corrosion. Electrochim Acta 46:3675–3683
52. Postlethwaite J (1981) Effect of chromate inhibitor on the mechanical and electrochemical components of erosion-corrosion in aqueous slurries of sand. Corrosion 37:1–5
53. Oltra R, Chapey B, Renaud L (1995) Abrasion–corrosion studies of passive stainless steels in acidic media: combination of acoustic emission and electrochemical techniques. Wear 186–187:533–541
54. Li W, Li DY (2005) Variations of work function and corrosion behaviour of deformed copper surfaces. Appl Surf Sci 240:388–395
55. Islam MA, Farhat ZN, Ahmed EM (2013) Erosion enhanced corrosion and corrosion enhanced erosion of API X-70 pipeline steel. Wear 302:1592–1601
56. Xie J, Alpas A, Northwood D (2003) The effect of erosion on the electrochemical properties of AISI 1020 steel. J Mater Eng Perform 12:77–86
57. Matsumura M, Oka Y, Hiura H, Yano M (1991) The role of passivating film in preventing slurry erosion-corrosion of austenitic stainless steel. ISIJ Int 31:168–172
58. Islam MA, Farhat ZN (2013) The synergistic effect between erosion and corrosion of API pipeline in CO_2 and saline medium. Tribol Int 68:26–34
59. Reyes M, Neville A (2001) Mechanisms of erosion-corrosion on a cobalt-base alloy and stainless-steel UNS S17400 in aggressive slurries. J Mater Eng Perform 10:723–730
60. Jones M, Waag U (2011) The influence of carbide dissolution on the erosion–corrosion properties of cast tungsten carbide/Ni-based PTAW overlays. Wear 271:1314–1324
61. Bester JA, Ball A (1993) The performance of aluminium alloys and particulate reinforced aluminium metal matrix composites in erosive-corrosive slurry environments. Wear 162–164:57–63
62. Zheng Y, Yao Z, Wei X, Ke W (1995) The synergistic effect between erosion and corrosion in acidic slurry medium. Wear 186–187:555–561
63. Gutman EM (1998) Mechanochemistry of materials. Cambridge International Science Publishing, UK
64. Lu BT, Luo JL, Lu JF (2004) Chemo-mechanical effect in erosion-corrosion process of carbon steel. Corrosion. Paper 04659
65. Li Y, Burstein T, Hutchings IM (1995) The influence of corrosion on the erosion of aluminium by aqueous silica slurries. Wear 186–187:515–522
66. Postlethwaite J, Brady BJ, Hawrylak MW, Tinker EB (1978) Effects of corrosion on the wear patterns in horizontal slurry pipelines. Corrosion 34:245–250

67. Hu X, Neville A (2009) CO_2 erosion-corrosion of pipeline steel (API X65) in oil and gas conditions-a systematic approach. Wear 267:2027–2032
68. Cao S, Maldonado SG, Mischler S (2015) Tribocorrosion of passive metals in the mixed lubrication regime: theoretical model and application to metal-on-metal artificial hip joints. Wear 324:55–63
69. Guadalupe S, Cao S, Cantoni M, Chitty W-J, Falcand C, Mischler S (2017) Applicability of a recently proposed tribocorrosion model to CoCr alloys with different carbides content. Wear 376:203–211
70. Landolt D, Mischler S, Stemp M (2001) Electrochemical methods in tribocorrosion: a critical appraisal. Electrochim Acta 46:3913–3929
71. Maldonado SG, Mischler S, Cantoni M, Chitty W-J, Falcand C, Hertz D (2013) Mechanical and chemical mechanisms in the tribocorrosion of a Stellite type alloy. Wear 308:213–221
72. Mischler S (2008) Triboelectrochemical techniques and interpretation methods in tribo-corrosion: a comparative evaluation. Tribol Int 41:573–583
73. Mischler S, Debaud S, Landolt D (1998) Wear-accelerated corrosion of passive metals in tribocorrosion systems. J Electrochem Soc 145:750–758
74. Mischler S, Munoz AI (2013) Wear of CoCrMo alloys used in metal-on-metal hip joints: a tribocorrosion appraisal. Wear 297:1081–1094
75. Gilbert JL, Mali SA, Liu Y (2016) Area-dependent impedance-based voltage shifts during tribocorrosion of Ti-6Al-4V biomaterials: theory and experiment. Surf Topogr 4:034002
76. Goldberg JR, Gilbert JL (1997) Electrochemical response of CoCrMo to high-speed fracture of its metal oxide using an electrochemical scratch test method. J Biomed Mater Res Part A 37:421–431
77. Swaminathan V, Gilbert JL (2012) Fretting corrosion of CoCrMo and Ti6Al4V interfaces. Biomaterials 33:5487–5503
78. Stachowiak A, Zwierzycki W (2012) Analysis of the tribocorrosion mechanisms in a pin-on-plate combination on the example of AISI304 steel. Wear 294–295:277–285
79. Stachowiak A, Zwierzycki W (2011) Tribocorrosion modeling of stainless steel in a sliding pair of pin-on-plate type. Tribol Int 44:1216–1224
80. Ghanbarzadeh Ali, Salehi Farnaz Motamen, Bryant Michael, Neville Anne (2019) A new asperity-scale mechanistic model of tribocorrosive wear: synergistic effects of mechanical wear and corrosion. J Tribol 141:021601
81. Jiaren Jiang, Stack MM (2006) Modelling sliding wear: from dry to wet environments. Wear 261:954–965
82. Jiang J, Stack MM, Neville A (2002) Modelling the tribocorrosion interaction in aqueous sliding conditions. Tribol Int 35:669–679
83. Zeng L, Zhang GA, Guo XP (2014) Erosion–corrosion at different locations of X65 carbon steel elbow. Corros Sci 85:318–330
84. Stack MM, Abdelrahman SM, Jana BD (2010) A new methodology for modelling erosion–corrosion regimes on real surfaces: gliding down the galvanic series for a range of metal-corrosion systems. Wear 268:533–542
85. Keating A, Nešić S (2001) Numerical prediction of erosion-corrosion in bends. Corrosion 57(7):621–633
86. Davis C, Frawley P (2009) Modelling of erosion–corrosion in practical geometries. Corros Sci 51:769–775
87. Wang H, Yang Yu, Jianxing Yu, Wang Z, Li H (2019) Development of erosion equation and numerical simulation methods with the consideration of applied stress. Tribol Int 137:387–404
88. Sundararajan G (1991) A comprehensive model for the solid particle erosion of ductile materials. Wear 149:111–127
89. Zum Gahr K-H (1988) Modelling of two body abrasive wear. Wear 124:87–103
90. Hokkirigawa K, Kato K (1988) The effect of hardness on the transition of abrasive wear mechanism of steels. Wear 123:241–251
91. Kato K (1997) Abrasive wear of metals. Tribol Int 30:333–338
92. Kitsunai H, Kato K, Hokkirigawa K, Inoue H (1990) The transitions between microscopic wear modes during repeated sliding friction observed by a scanning electron microscope tribosystem. Wear 135:237–249
93. Jiang J, Arnell RD (1998) The dependence of the fraction of material removed on the degree of penetration in single particle abrasion of ductile materials. J Phys D 31:1163–1167
94. Raicheff RG, Damajanovic A, Bockris JOM (1967) Dependence of the velocity of the anodic dissolution of iron on its yield rate under tension. J Chem Phys 47:2198–2217
95. Keddam M, Silva JVD (1980) The influence of straining on the anodic behaviour of iron in an acidic medium. Corros Sci 20:167–175
96. Johnson KL (1985) Contact mechanics. Cambridge University Press, Cambridge, p 361
97. Ma Liang, Huang Cheng, Xie Yongsong, Jiaren Jiang KY, Tufa Rob Hui, Liu Z-S (2015) Modeling of erodent particle trajectories in slurry flow. Wear 334–335:49–55
98. Finnie I (1960) Erosion of surfaces by solid particles. Wear 3:87–103
99. Finnie I (1972) Some observations on the erosion of ductile metals. Wear 19:81–90
100. Bitter JGA (1963) A study of erosion phenomena—part I. Wear 6:5–21
101. Bitter JGA (1963) A study of erosion phenomena—part II. Wear 6:169–190
102. Ghanbarzadeh Ali, Salehi Farnaz Motamen, Bryant Michael, Neville Anne (2019) Modelling the evolution of electrochemical current in potentiostatic condition using an asperity-scale model of tribocorrosion. Biotribology 17:19–29
103. Kaesche H (2003) Corrosion of metals: physicochemical principles and current problems, 4th edn. Springer, Heidelberg, p 1
104. Marcus P (ed) (2017) Corrosion mechanisms in theory and practice, 3rd edn. Taylor and Francis, New York
105. Bronson A, Nelson J, Kang C (1992) Analysis of the scribing technique for determining the corrosion wear of an Fe-21wt% Ni alloy. Wear 154:387–401
106. Wang XY, Li DY (2001) Investigation of the synergism of wear and corrosion using an electrochemical scratch technique. Tribol Lett 11:117–120
107. Dalbert V, Mary N, Normand B, Verdu C, Saedlou S (2020) In situ determinations of the wear surfaces, volumes and kinetics of repassivation: contribution in the understanding of the tribocorrosion behaviour of a ferritic stainless steel in various pH. Tribol Int 150:106374
108. Olsson Claes-Olof A, Munoz Anna Neus Igual, Cao Shoufan, Mischler Stefano (2021) Modeling current transients in a reciprocal motion tribocorrosion experiment. J Electrochem Soc 168:031503
109. Mary N, Ter-Ovanessian B, Normand B (2020) Growth mechanism and repassivation kinetic determinations on stainless steel under sliding: role of the solution pH and dissolved oxygen concentration. Wear 460–461:203478
110. Hoar TP, Ford FP (1973) Electrode reaction rates on straining aluminum-magnesium wires in chloride and sulfate solutions. J Electrochem Soc 120:1013
111. Jiaren (Jimmy) Jiang, MD Aminul Islam, Yongsong Xie, Baisheng Yao (2021) On the suitability of ASTM 532 IIB Cr white cast irons for erosion-corrosion and abrasion-corrosion applications, Corrosion. Paper Number: NACE-2021–17018. Published: April 19 2021
112. Postlethwaite J, Tinker EB, Hawrylak MW (1974) Erosion-corrosion in slurry pipelines. Corrosion 30:285–289

113. Md Aminul Islam, Jiaren (Jimmy) Jiang, Yongsong Xie (2021) Erosion-corrosion assessment of Cr white irons. Corrosion. Paper Number: NACE-2021–16478. Published: April 19 2021